From photonic crystals to metamaterials: the bianisotropic response

New Journal of Physics
The open-access journal for physics

From photonic crystals to metamaterials: the bianisotropic response

J A Reyes-Avendaño[1], U Algredo-Badillo[1], P Halevi[1,3] and F Pérez-Rodríguez[2]

[1] Instituto Nacional de Astrofísica, Óptica y Electrónica, Apartado Postal 51, Puebla, Pue. 72000, Mexico

[2] Instituto de Física, Benemérita Universidad Autónoma de Puebla, Apartado Postal J-48, Puebla, Pue. 72570, Mexico

E-mail: halevi@inaoep.mx

New Journal of Physics **13** (2011) 073041 (33pp)
Received 31 January 2011
Published 29 July 2011
Online at http://www.njp.org/
doi:10.1088/1367-2630/13/7/073041

Abstract. Metamaterials are, in general, characterized by the *bianisotropic response* that relates the displacement vector **D** and the magnetic induction **B** to the electric and magnetic fields **E** and **H** via the permittivity, permeability and magnetoelectric dyadics, respectively, $\overleftrightarrow{\boldsymbol{\varepsilon}}$, $\overleftrightarrow{\boldsymbol{\mu}}$ and $\overleftrightarrow{\boldsymbol{\gamma}}$ $(= -\overleftrightarrow{\boldsymbol{\delta}}_T)$. For the first time, we derived these dyadics with great generality with the photonic crystal (PC) description as the starting point. The PC can have one- (1D), two- (2D) or three-dimensional (3D) periodicity with an arbitrary Bravais lattice and arbitrary shape of the inclusions in the unit cell, and these inclusions can be dielectric or metallic. Moreover, unlike most theories of homogenization, our theory is, in principle, applicable to band-pass or optical bands, as well as to low-pass or acoustic bands. The generalized conductivity $\hat{\sigma}(\mathbf{r})$ is assumed to be given at every point in the unit cell, and we relate $\overleftrightarrow{\boldsymbol{\varepsilon}}$, $\overleftrightarrow{\boldsymbol{\mu}}$ and $\overleftrightarrow{\boldsymbol{\gamma}}$ analytically to $\hat{\sigma}(\mathbf{r})$. The long-wavelength limit having been taken, these dyadics depend only on the direction of the Bloch wave vector **k** and not on its magnitude. In the case of inversion symmetry, the bianisotropic response simplifies to $\mathbf{D} = \overleftrightarrow{\boldsymbol{\varepsilon}} \cdot \mathbf{E}$ and $\mathbf{B} = \overleftrightarrow{\boldsymbol{\mu}} \cdot \mathbf{H}$. Applying our theory to a 2D array of metallic wires, we find that the response is paramagnetic or diamagnetic, depending on whether it is the electric or the magnetic field that is parallel to the wires. For a 3D array of mutually perpendicular wires (3D crosses), the behavior is found to change from plasma-like to free-photon-like when the wires are severed, leading to a spectral region where ε and μ are both negative. Finally, our theory confirms several well-known results for particular PCs and inclusions.

[3] Author to whom any correspondence should be addressed.

Contents

1. Introduction

Over the last 30 years, photonic crystals (PCs) have been intensively studied because they offer the possibility of controlling the flow of light [1]. The way in which these artificial periodic structures interact with an electromagnetic wave strongly depends on the ratio between the lattice constant a and the electromagnetic wavelength λ. When $\lambda \lessapprox a$, light traveling through the PC experiences strongly the dielectric contrast between the different materials forming the periodic structure, in the same way as electrons 'feel' the periodic potential in a semiconductor crystal. For a sufficiently strong dielectric contrast and an appropriate choice of geometric parameters, it is possible to obtain artificial materials possessing a frequency region in which light cannot propagate through the structure. This region is usually called photonic band gap (PBG). Improved mirrors, wave guides, optical switches and lasers [2–5], among other applications, have been developed by taking advantage of this PBG region. On the other hand, when $\lambda \gg a$, another situation is observed. Long-wavelength light traveling through the structure does not experience the details of the structure of the artificial material and the PC behaves as if it were homogeneous. Therefore, the optical properties can be described well by employing Maxwell's equations for the average electromagnetic fields together with macroscopic constitutive relations [6, 7]. In this frequency region (long-wavelength limit),

PCs are used as conventional optical devices such as lenses, prisms or polarizers but with unusual behavior. The properties of PCs can be custom-tailored by suitable selection of their parameters [8–10].

Since the papers by Smith and collaborators [11–13] demonstrating the existence of arrays of conducting elements possessing a negative effective refractive index (corresponding to negative permittivity and negative permeability in the same range of frequency), the number of papers dealing with PCs in the long-wavelength limit has grown exponentially. The idea of negative refraction has a very interesting history, recently reviewed by Agranovich and Gartstein [14]. The idea can be traced back to the mention of such a possibility by Schuster [15] in 1909 and a thorough analysis by Mandel'shtam [16] in 1945, also published later in book form [17]. More recently, negative refraction was discussed by Sivukhin [18] and by Pafomov [19–21], to be finally rediscovered by Veselago [22]. Many years later, Pendry and collaborators [23, 24] showed that negative-index materials are viable in practice. New kinds of materials, called *metamaterials*, opened the door to an entirely new field in optics, where Snell's law applies with a negative index of refraction. Consequently, a large body of work has been devoted to the development of theoretical and numerical methods that can predict the effective permittivity, permeability, etc of metamaterials, leading to convenience in understanding and designing these interesting structures.

Numerous works are dedicated to mean-field theories for selected types of PCs, using miscellaneous approximations, such as the Lorentz approach [25], the Clausius–Mosotti method [26], the Maxwell–Garnett approximation [27], the spectral representation method [28] and transmission line studies [29]. Further, several homogenization theories have focused on arbitrary dielectric [10, 30–32] or metallic [33–34] inclusions in the long-wavelength limit. The aforementioned homogenization theories all limit the generality to one or more of the following aspects: the form of the inclusion, type of material, filling fraction and photonic band.

Also available are two approaches to homogenization that are of much wider generality: the effective parameter retrieval (EPR) method and the field averaging (FA) method. The EPR method [35–41] determines the effective parameters, $\varepsilon(\omega)$ and $\mu(\omega)$, by requiring that the scattering spectra of an inhomogeneous medium slab coincide with those of the corresponding homogeneous medium. On the other hand, the FA method is based on the averaging of the PC's electromagnetic fields in a unit cell. Initiated by Pendry and collaborators, it has been inspired by finite-difference solutions of Maxwell's equations [24, 42–44]. Both the EPR method and the FA method are numerical methods for the determination of effective parameters, rather than mean-field (homogenization) theories. An approach similar to FA has been used by Silveirinha and Fernandes [45–47] for the case of wire media. More recently, Silveirinha [48] proposed a source-driven approach to homogenization, leading to an integral equation that can be solved in closed form for the effective dielectric tensor $\overleftrightarrow{\boldsymbol{\varepsilon}}(\mathbf{k})$. This led to generalized Lorentz–Lorenz formulae [49] and to numerical implementation (by a finite-difference frequency-domain method) of the aforementioned approach [50]. Căbuz *et al* [51] developed a two-step approach to homogenization whereby first a layer of wires or resonators is homogenized as a slab, followed by homogenization of the resulting stack of layers. We also note that homogenization theories are available for nonperiodic (random) media as well [52–54]. The very general dielectric homogenization theory of Mochán and Barrera [54] was recently adapted to periodic PCs [55]. In the latter paper by Ortiz *et al* [55], the effective dielectric tensor is derived by a method of projection operators. We note that the expressions for $\overleftrightarrow{\boldsymbol{\varepsilon}}(\mathbf{k})$ in [48] and [45] are equivalent to ours *for the dielectric response*, rather

than the *bianisotropic* response. The latter response was also studied by a numerical current-driven approach [56].

There exist, in principle, many ways of defining the effective parameters by suitably relating the macroscopic constitutive fields, namely the dielectric displacement $\mathbf{D}$ and the magnetic field $\mathbf{H}$, to the physical macroscopic fields, namely the electric field $\mathbf{E}$ and the magnetic induction $\mathbf{B}$. Perhaps the most general linear constitutive relation is the so-called bianisotropic response [37, 52, 57–60]

$$\mathbf{D} = \overleftrightarrow{\boldsymbol{\varepsilon}} \cdot \mathbf{E} + \overleftrightarrow{\boldsymbol{\gamma}} \cdot \mathbf{H}, \quad \mathbf{B} = \overleftrightarrow{\boldsymbol{\delta}} \cdot \mathbf{E} + \overleftrightarrow{\boldsymbol{\mu}} \cdot \mathbf{H}.$$

On the other hand, in nominally nonmagnetic media (especially in solid state physics and in crystal optics), it is common to take into account *small* magnetic effects by employing only a *nonlocal* effective dielectric tensor $\overleftrightarrow{\boldsymbol{\varepsilon}}(\mathbf{k})$ [53, 58, 61–63],

$$\mathbf{D} = \overleftrightarrow{\boldsymbol{\varepsilon}}(\mathbf{k}) \cdot \mathbf{E}, \quad \mathbf{B} = \mu_0 \mathbf{H}.$$

Because these magnetic effects are small—unlike the usual situation with metamaterials—it is convenient to 'hide' them in the wavevector dependence of the effective dielectric tensor. Furthermore, because of the smallness of the a/λ ratio, the effects of spatial dispersion, which can be associated with the magnetic field, turn out to be rather weak.

In this paper, we present a mean-field theory of PCs that goes beyond conventional ones. This is a theory for an unbounded PC, an abstraction made in the tradition of crystal optics theories for a bulk medium [61]. By assuming that the Bloch wavelength is much greater than the lattice constant of the periodic artificial structure, we derive analytic results on the effective tensors of both the bianisotropic response ($\overleftrightarrow{\boldsymbol{\varepsilon}}, \overleftrightarrow{\boldsymbol{\gamma}}, \overleftrightarrow{\boldsymbol{\delta}}, \overleftrightarrow{\boldsymbol{\mu}}$) and the nonlocal dielectric response ($\overleftrightarrow{\boldsymbol{\varepsilon}}(\mathbf{k})$). These are determined for arbitrary periodicity (one- (1D), two- (2D) or three-dimensional (3D)) of the PC, for an arbitrary Bravais lattice and for arbitrary structure of the unit cell. Considering isotropic and nonmagnetic materials in the unit cell of the photonic crystal, we show that the use of the bianisotropic response allows us to distinguish clearly the magnetic effects and, consequently, to characterize more properly the electromagnetic metamaterial properties. This paper derives the bianisotropic response from the PC or 'micro-level', for the first time on the basis of a very general set of assumptions. The effective permittivity and permeability for specific dielectric and metallo-dielectric photonic crystals are calculated, analyzed and, in some cases, compared with other theories in the literature.

The paper is organized as follows. In section 2, we describe our general approach to homogenization, from which both the dielectric response (section 3) and the bianisotropic response (section 4) are derived. In section 5, we present the corresponding dispersion relation for the homogenized medium. Section 6 is devoted to an analysis of some important special cases in which the general formulae are simplified and reduced to analytical results. In section 7, we give numerical results for two simple systems that are compared with other works, and we present the effective permittivity and permeability spectra for a few metallo-dielectric structures that exhibit metamaterial behavior. The conclusions are given in section 8. Finally, the proofs of several formulae have been relegated to the appendices.

2. Mean-field theory

Let us consider a boundless PC composed, in general, of metallic and dielectric components. The form of the inclusions in the unit cell and the Bravais lattice are assumed to be completely

arbitrary. In addition, the inclusions can be either isolated or in contact. For simplicity, we also assume that the component materials are isotropic and that the metal has no magnetic properties. Such a PC can be described by only a single material scalar field, namely the position-dependent generalized conductivity[4],

$$\hat{\sigma}(\mathbf{r}) = \sigma(\mathbf{r}) - \mathrm{i}\omega\varepsilon_0\chi(\mathbf{r}), \tag{1}$$

having the same periodicity as the PC. $\sigma(\mathbf{r})$ and $\chi(\mathbf{r})$ in equation (1) are, correspondingly, the usual conductivity and susceptibility for isotropic materials in the unit cell. We note that in equation (1) a metallic component is usually characterized by $\chi(\mathbf{r}) = 0$, while a dielectric component is described by $\sigma(\mathbf{r}) = 0$. For vacuum both $\sigma(\mathbf{r})$ and $\chi(\mathbf{r})$ vanish; thus $\hat{\sigma}(\mathbf{r}) = 0$. Hence, our description covers both metallo-dielectric and dielectric PCs. In the following, we use the term 'micro-level' to define the PC level of description in which the inhomogeneous medium is described by the position-dependent conductivity equation (1). On the other hand, the term 'macro-level' is used in the long-wavelength limit when the structure is described by position-independent effective parameters. The macro-level thus corresponds to an effectively uniform—but not necessarily isotropic—medium, called 'metamaterial' if possessing unusual properties.

The electromagnetic fields inside the PC are governed by Maxwell's equations at the 'micro-level', which, according to our assumptions, can be written in the form [7]

$$\nabla \times \mathbf{b}(\mathbf{r}) = \mu_0\mathbf{j}(\mathbf{r}) - \mu_0\,\mathrm{i}\omega\varepsilon_0\mathbf{e}(\mathbf{r}), \tag{2}$$

$$\nabla \cdot \mathbf{e}(\mathbf{r}) = -\frac{\mathrm{i}}{\varepsilon_0\omega}\nabla \cdot \mathbf{j}(\mathbf{r}), \tag{3}$$

$$\nabla \times \mathbf{e}(\mathbf{r}) = \mathrm{i}\omega\mathbf{b}(\mathbf{r}), \tag{4}$$

$$\nabla \cdot \mathbf{b}(\mathbf{r}) = 0. \tag{5}$$

Here, the requirement of charge conservation ($\mathrm{i}\omega\rho = \nabla \cdot \mathbf{j}$) has been used, the fields are proportional to $\exp(-\mathrm{i}\omega t)$, MKS units are employed, and the current density $\mathbf{j}$ is

$$\mathbf{j}(\mathbf{r}) = \hat{\sigma}(\mathbf{r})\mathbf{e}(\mathbf{r}). \tag{6}$$

By equation (6), this current density is produced by the electric field $\mathbf{e}(\mathbf{r})$ of the PC that, in turn, is supposed to be the consequence of some virtual, unspecified excitation.

Because of the periodicity, the generalized conductivity can be expanded in a Fourier series,

$$\hat{\sigma}(\mathbf{r}) = \sum_{\mathbf{G}} \hat{\sigma}(\mathbf{G})\mathrm{e}^{\mathrm{i}\mathbf{G}\cdot\mathbf{r}}, \tag{7}$$

and the 'micro-level' fields $\mathbf{e}(\mathbf{r})$ and $\mathbf{b}(\mathbf{r})$ obey the Bloch theorem. Hence,

$$\mathbf{e}(\mathbf{r}) = \sum_{\mathbf{G}} \mathbf{e}(\mathbf{G})\,\mathrm{e}^{\mathrm{i}(\mathbf{k}+\mathbf{G})\cdot\mathbf{r}} = \mathbf{e}(\mathbf{G}=0)\,\mathrm{e}^{\mathrm{i}\mathbf{k}\cdot\mathbf{r}} + \sum_{\mathbf{G}}{}' \mathbf{e}(\mathbf{G})\,\mathrm{e}^{\mathrm{i}(\mathbf{k}+\mathbf{G})\cdot\mathbf{r}}, \tag{8}$$

$$\mathbf{b}(\mathbf{r}) = \sum_{\mathbf{G}} \mathbf{b}(\mathbf{G})\,\mathrm{e}^{\mathrm{i}(\mathbf{k}+\mathbf{G})\cdot\mathbf{r}} = \mathbf{b}(\mathbf{G}=0)\,\mathrm{e}^{\mathrm{i}\mathbf{k}\cdot\mathbf{r}} + \sum_{\mathbf{G}}{}' \mathbf{b}(\mathbf{G})\,\mathrm{e}^{\mathrm{i}(\mathbf{k}+\mathbf{G})\cdot\mathbf{r}}, \tag{9}$$

[4] Equation (1) for the generalized or complex conductivity is obtained from the Ampére–Maxwell law, by writing $\nabla \times \mathbf{H} = \mathbf{j} - \mathrm{i}\omega\mathbf{D} = \sigma\mathbf{E} - \mathrm{i}\omega(1+\chi)\varepsilon_0\mathbf{E} = (\sigma - \mathrm{i}\omega\chi\varepsilon_0)\mathbf{E} - \mathrm{i}\omega\varepsilon_0\mathbf{E} \equiv \hat{\sigma}\mathbf{E} - \mathrm{i}\omega\varepsilon_0\mathbf{E}$.

where the primes indicate that the term with $\mathbf{G} = 0$ is excluded from the sums. Here $\mathbf{k}$ is the Bloch wave vector in the case of a 3D PC. However, for 2D (1D) PCs, the wave vector $\mathbf{k}$ may also have a wave vector component in a direction parallel to the cylinders (interfaces) that is not a Bloch vector.

For Bloch wavelengths $2\pi/k$ much larger than the lattice constant a,

$$ka \ll 1, \tag{10}$$

and in the case of 3D periodicity the 'macro-level' electric field $\mathbf{E}(\mathrm{r})$ and magnetic induction $\mathbf{B}(\mathrm{r})$ can be obtained by averaging the micro-level fields $\mathbf{e}(\mathrm{r})$ (equation (8)) and $\mathbf{b}(\mathrm{r})$ (equation (9)) over a spherical volume of radius R much larger than a, but much smaller than the wavelength $2\pi/k$ ($a \ll R \ll 2\pi/k$). This averaging procedure smoothes out the rapid oscillations of the micro-level fields inside the volume of the chosen radius R. The rapid oscillations are described by the terms with $\mathbf{G} \neq 0$ in equations (8) and (9). Therefore,

$$\mathbf{E}(\mathbf{r}) \equiv \langle \mathbf{e}(\mathbf{r}) \rangle = \mathbf{e}(\mathbf{G} = 0)\, \mathrm{e}^{\mathrm{i}\mathbf{k}\cdot\mathbf{r}} = \mathbf{E}_0\, \mathrm{e}^{\mathrm{i}\mathbf{k}\cdot\mathbf{r}}, \tag{11}$$

$$\mathbf{B}(\mathbf{r}) \equiv \langle \mathbf{b}(\mathbf{r}) \rangle = \mathbf{b}(\mathbf{G} = 0)\, \mathrm{e}^{\mathrm{i}\mathbf{k}\cdot\mathbf{r}} = \mathbf{B}_0\, \mathrm{e}^{\mathrm{i}\mathbf{k}\cdot\mathbf{r}}, \tag{12}$$

where $\langle \ldots \rangle$ indicates volumetric averaging. It is significant that, as a consequence of our averaging procedure, for 3D periodicity the Bloch wave vector became the ordinary wave vector of a plane wave in equations (11) and (12). In the case of 2D (1D) periodicity, the averaging is performed within a circle (segment). In these cases k in equation (10) is the magnitude of the total wave vector that includes, in addition to the Bloch vector, possible parallel components, as noted after equation (9).

The Maxwell equations for the fields at the macro-level are derived by averaging the micro-level equations (2)–(5). We obtain

$$\mathbf{k} \times \mathbf{B} = -\mathrm{i}\mu_0 \langle \mathbf{j} \rangle - \mu_0 \omega \varepsilon_0 \mathbf{E}, \tag{13}$$

$$\mathbf{k} \cdot \mathbf{E} = -\frac{\mathrm{i}}{\varepsilon_0 \omega} \mathbf{k} \cdot \langle \mathbf{j} \rangle\,, \tag{14}$$

$$\mathbf{k} \times \mathbf{E} = \omega \mathbf{B}, \tag{15}$$

$$\mathbf{k} \cdot \mathbf{B} = 0. \tag{16}$$

In obtaining equations (13)–(16), we took into account the fact that the derivatives and the averaging commute [6, 7].

Now, in order to determine the material equation for the homogenized photonic crystal, it is necessary to establish the relation between the macroscopic current density $\langle \mathbf{j} \rangle = \mathbf{j}_0 \exp(\mathrm{i}\mathbf{k} \cdot \mathbf{r})$ and the electric field $\mathbf{E}(\mathbf{r})$ (equation (11)). As follows from equations (6) and (7), the amplitude $\mathbf{j}_0$ can be written as

$$\mathbf{j}_0 = \hat{\sigma}(\mathbf{G} = 0)\mathbf{e}(\mathbf{G} = 0) + {\sum_{\mathbf{G}}}' \hat{\sigma}(-\mathbf{G})\mathbf{e}(\mathbf{G}). \tag{17}$$

To express the quantities $\mathbf{e}(\mathbf{G} \neq 0)$ in terms of $\mathbf{e}(\mathbf{G} = 0)$, we use the wave equation

$$\nabla \times \nabla \times \mathbf{e}(\mathbf{r}) = \left[\mathrm{i}\mu_0 \omega \hat{\sigma}(\mathbf{r}) + k_0^2\right] \mathbf{e}(\mathbf{r}), \tag{18}$$

which is obtained by eliminating the magnetic induction $\mathbf{b}(\mathbf{r})$ from the Ampére–Maxwell law equation (2) and Faraday's law equation (4) with $k_0^2 = \mu_0\varepsilon_0\omega^2$. Then, we substitute equations (8) and (7) into equation (18) and finally obtain

$$(\mathbf{k}+\mathbf{G}) \times (\mathbf{k}+\mathbf{G}) \times \mathbf{e}(\mathbf{G}) + k_0^2\mathbf{e}(\mathbf{G}) = -\mathrm{i}\omega\mu_0 \sum_{\mathbf{G}'} \hat{\sigma}(\mathbf{G}-\mathbf{G}')\mathbf{e}(\mathbf{G}'). \tag{19}$$

This equation can be rewritten in dyadic notation as

$$\sum_{\mathbf{G}'}{}' \overleftrightarrow{\mathbf{M}}(\mathbf{k};\mathbf{G},\mathbf{G}') \cdot \mathbf{e}(\mathbf{G}') = \mathrm{i}\omega\mu_0\hat{\sigma}(\mathbf{G})\mathbf{e}(0), \quad \mathbf{G} \neq 0, \tag{20}$$

where the dyadic $\overleftrightarrow{\mathbf{M}}(\mathbf{k};\mathbf{G},\mathbf{G}')$ is defined for $\mathbf{G} \neq 0$ and $\mathbf{G}' \neq 0$ as

$$\overleftrightarrow{\mathbf{M}}(\mathbf{k};\mathbf{G},\mathbf{G}') = [(|\mathbf{k}+\mathbf{G}|^2 - k_0^2)\overleftrightarrow{\mathbf{I}} - (\mathbf{k}+\mathbf{G})(\mathbf{k}+\mathbf{G})]\delta_{\mathbf{G},\mathbf{G}'} - \mathrm{i}\omega\mu_0\hat{\sigma}(\mathbf{G}-\mathbf{G}')\overleftrightarrow{\mathbf{I}}. \tag{21}$$

Here, $\overleftrightarrow{\mathbf{I}}$ and $\delta_{\mathbf{G},\mathbf{G}'}$ are, respectively, the unit dyadic and the Kronecker delta. Solving equation (20) for $\mathbf{e}(\mathbf{G} \neq 0)$, we find the expression

$$\mathbf{e}(\mathbf{G}) = \mathrm{i}\omega\mu_0 \sum_{\mathbf{G}'}{}' \overleftrightarrow{\mathbf{M}}^{-1}(\mathbf{k};\mathbf{G},\mathbf{G}')\hat{\sigma}(\mathbf{G}') \cdot \mathbf{e}(0), \quad \mathbf{G} \neq 0. \tag{22}$$

After substituting this expression into equation (17), we finally obtain the macroscopic current density in the form

$$\mathbf{j}_0 = \overleftrightarrow{\boldsymbol{\Sigma}}(\mathbf{k}) \cdot \mathbf{E}_0, \tag{23}$$

where $\overleftrightarrow{\boldsymbol{\Sigma}}(\mathbf{k})$ is the effective conductivity dyadic:

$$\overleftrightarrow{\boldsymbol{\Sigma}}(\mathbf{k}) = \hat{\sigma}(\mathbf{G}=0)\overleftrightarrow{\mathbf{I}} + \mathrm{i}\omega\mu_0 \sum_{\mathbf{G},\mathbf{G}'}{}' \hat{\sigma}(-\mathbf{G})\overleftrightarrow{\mathbf{M}}^{-1}(\mathbf{k};\mathbf{G},\mathbf{G}')\hat{\sigma}(\mathbf{G}'). \tag{24}$$

We have also derived an equivalent formula for $\overleftrightarrow{\boldsymbol{\Sigma}}(\mathbf{k})$, which can be written as

$$\overleftrightarrow{\boldsymbol{\Sigma}}(\mathbf{k}) = \frac{\mathrm{i}}{\omega\mu_0}\left[\{\overleftrightarrow{\mathbf{N}}^{-1}(\mathbf{k};0,0)\}^{-1} - \left(k^2 - k_0^2\right)\overleftrightarrow{\mathbf{I}} + \mathbf{kk}\right], \tag{25}$$

where $\overleftrightarrow{\mathbf{N}}(\mathbf{k};\mathbf{G},\mathbf{G}')$ is given by equation (21) ($\overleftrightarrow{\mathbf{N}}(\mathbf{k};\mathbf{G},\mathbf{G}') = \overleftrightarrow{\mathbf{M}}(\mathbf{k};\mathbf{G},\mathbf{G}')$); now however, $\mathbf{G}$ and $\mathbf{G}'$ range over all the vectors of the reciprocal lattice (i.e. including $\mathbf{G}=0$ and $\mathbf{G}'=0$). The last equation may be more convenient from the computational point of view because the double sum in equation (24) is avoided and only one 3×3 matrix block of the inverse matrix $\overleftrightarrow{\mathbf{N}}^{-1}(\mathbf{k};\mathbf{G},\mathbf{G}')$ must be obtained. The derivation of equation (25) is given in appendix A.

Employing equation (24) or (25), substitution of equation (23) into Maxwell's equations (13)–(16) gives

$$\mathbf{k} \times \mathbf{B}_0 = -\mu_0[\omega\varepsilon_0\overleftrightarrow{\mathbf{I}} + \mathrm{i}\overleftrightarrow{\boldsymbol{\Sigma}}(\mathbf{k})] \cdot \mathbf{E}_0, \tag{26}$$

$$\mathbf{k} \cdot [\omega\varepsilon_0\overleftrightarrow{\mathbf{I}} + \mathrm{i}\overleftrightarrow{\boldsymbol{\Sigma}}(\mathbf{k})] \cdot \mathbf{E}_0 = 0, \tag{27}$$

$$\mathbf{k} \times \mathbf{E}_0 = \omega\mathbf{B}_0, \tag{28}$$

$$\mathbf{k} \cdot \mathbf{B}_0 = 0. \tag{29}$$

Equations (26)–(29), with the conductivity dyadic $\overleftrightarrow{\boldsymbol{\Sigma}}(\mathbf{k})$ given by equation (24), are the starting point for the derivation of specific forms of the effective or macro-level material responses that relate the auxiliary fields $\mathbf{D}$ and $\mathbf{H}$ to the physical fields $\mathbf{E}$ and $\mathbf{B}$. In the next section we impose the requirement that the effective medium has no magnetic properties, thus leading to a purely dielectric response. On the other hand, in section 4 we assume that the effective response is bianisotropic: namely, in general the field $\mathbf{D}$ depends on $\mathbf{H}$ (in addition to $\mathbf{E}$) and the field $\mathbf{B}$ depends on $\mathbf{E}$ (in addition to $\mathbf{H}$).

3. Dielectric response

A very convenient way of determining the effective material response is to compare the average Maxwell equations, derived in the preceding section (see equations (26)–(29)), with the corresponding equations for a macroscopic homogeneous medium:

$$\mathbf{k} \times \mathbf{H} = -\omega \mathbf{D}, \tag{30}$$

$$\mathbf{k} \cdot \mathbf{D} = 0, \tag{31}$$

$$\mathbf{k} \times \mathbf{E} = \omega \mathbf{B}, \tag{32}$$

$$\mathbf{k} \cdot \mathbf{B} = 0. \tag{33}$$

Hence, we should define the relation between the auxiliary fields $\mathbf{D}$ and $\mathbf{H}$ and the physical fields $\mathbf{E}$ and $\mathbf{B}$. However, the form of the material response is *not* unique. One of the possibilities is to write the constitutive relations as [61–63]

$$\mathbf{D} = \overleftrightarrow{\boldsymbol{\varepsilon}}(\mathbf{k}, \omega) \cdot \mathbf{E}, \tag{34}$$

$$\mathbf{B} = \mu_0 \mathbf{H}. \tag{35}$$

This choice, evidently, does not take into account explicitly the magnetic effects. The electromagnetic properties of the homogeneous material depend only on the form of the wave vector-dependent, in general, dielectric dyadic $\overleftrightarrow{\boldsymbol{\varepsilon}}(\mathbf{k}, \omega)$. If we substitute equations (34) and (35) into (30) and (31), comparison with equations (26) and (27) shows that this dyadic is

$$\overleftrightarrow{\boldsymbol{\varepsilon}}(\mathbf{k}, \omega) = \varepsilon_0 \overleftrightarrow{\mathbf{I}} + \frac{\mathrm{i}}{\omega} \overleftrightarrow{\boldsymbol{\Sigma}}(\mathbf{k}, \omega), \tag{36}$$

with $\overleftrightarrow{\boldsymbol{\Sigma}}(\mathbf{k}, \omega)$ given by equations (24) and (21).

Now, although the derivation from equation (17) to equation (24) does not involve any approximation, our mean-field approach relies on the smallness of k, namely equation (10). For this reason, it makes sense to expand $\overleftrightarrow{\boldsymbol{\Sigma}}(\mathbf{k}, \omega)$ in powers of the small parameter ka:

$$\overleftrightarrow{\boldsymbol{\Sigma}}(\mathbf{k}) = \overleftrightarrow{\boldsymbol{\Sigma}}^{(0)} + k \overleftrightarrow{\boldsymbol{\Sigma}}^{(1)}(\hat{\mathbf{k}}) + k^2 \overleftrightarrow{\boldsymbol{\Sigma}}^{(2)}(\hat{\mathbf{k}}) + \cdots. \tag{37}$$

Note that the dyadics $\overleftrightarrow{\boldsymbol{\Sigma}}^{(1)}$ and $\overleftrightarrow{\boldsymbol{\Sigma}}^{(2)}$, although independent of the magnitude of $\mathbf{k}$, do depend on its direction, namely on the unit vector $\hat{\mathbf{k}} = \mathbf{k}/k$. Regarding the frequency ω, which is considered independent of $\mathbf{k}$ in expanding $\overleftrightarrow{\boldsymbol{\Sigma}}(\mathbf{k}, \omega)$ (37), it must also be small enough ($\omega \ll 2\pi c/a$).

In the next section, we will derive the effective conductivity dyadic $\overleftrightarrow{\boldsymbol{\Sigma}}(\mathbf{k}, \omega)$ (24) in the quadratic approximation, equation (37). This, of course, also determines the dielectric tensor

$\overleftrightarrow{\boldsymbol{\varepsilon}}(\mathbf{k}, \omega)$ (equation (36)) of the dielectric response in the same order of $\mathbf{k}$. In particular, in the long-wavelength limit, the resulting expression $\overleftrightarrow{\boldsymbol{\varepsilon}}(\mathbf{k} \to 0,\ \omega \to 0)$ from our formulae correctly yields the effective dielectric function, calculated previously for 3D [31] and 2D [10, 32] dielectric PCs. In addition, the expression obtained here for the effective permittivity tensor $\overleftrightarrow{\boldsymbol{\varepsilon}}(\mathbf{k}, \omega)$ is consistent with the results of [60] in the case of nonmagnetic dielectric PCs. The dyadic $\overleftrightarrow{\boldsymbol{\Sigma}}$ will also lead us to relate the bianisotropic response to the PC 'micro-level'.

4. Bianisotropic response

There exists another form, called bianisotropic, for expressing the material response of the homogenized material. The bianisotropic response establishes the relation between $\mathbf{D}$, $\mathbf{H}$, $\mathbf{E}$ and $\mathbf{B}$ by employing four dyadics:

$$\mathbf{D} = \overleftrightarrow{\boldsymbol{\varepsilon}} \cdot \mathbf{E} + \overleftrightarrow{\boldsymbol{\gamma}} \cdot \mathbf{H}, \tag{38}$$

$$\mathbf{B} = \overleftrightarrow{\boldsymbol{\delta}} \cdot \mathbf{E} + \overleftrightarrow{\boldsymbol{\mu}} \cdot \mathbf{H}. \tag{39}$$

Here, $\overleftrightarrow{\boldsymbol{\varepsilon}}$ is the permittivity, $\overleftrightarrow{\boldsymbol{\mu}}$ is the permeability and $\overleftrightarrow{\boldsymbol{\gamma}}$ and $\overleftrightarrow{\boldsymbol{\delta}}$ are the 'crossed' magneto-electric dyadics.

To derive the bianisotropic material response in the long-wavelength limit, we use the expansion of the effective conductivity dyadic $\overleftrightarrow{\boldsymbol{\Sigma}}(\mathbf{k})$, equation (37). Below, we consider only the first three terms of equation (37). The reason for this is that higher-order terms would lead to k-dependent corrections in the dyadic parameters of equations (38) and (39)—outside the scope of the present paper. By equation (24), the zero-order term is

$$\overleftrightarrow{\boldsymbol{\Sigma}}^{(0)} = \overleftrightarrow{\boldsymbol{\Sigma}}(0) = \hat{\sigma}(\mathbf{G} = 0)\overleftrightarrow{\mathbf{I}} + \mathrm{i}\omega\mu_0 {\sum_{\mathbf{G}}}' \hat{\sigma}(\mathbf{G})\overleftrightarrow{\mathbf{C}}_1(\mathbf{G}), \tag{40}$$

$$\overleftrightarrow{\mathbf{C}}_1(\mathbf{G}) = {\sum_{\mathbf{G}'}}' \hat{\sigma}(-\mathbf{G}')\overleftrightarrow{\mathbf{M}}_0^{-1}(\mathbf{G}', \mathbf{G}), \tag{41}$$

where, by equation (21),

$$\overleftrightarrow{\mathbf{M}}_0(\mathbf{G}, \mathbf{G}') \equiv \overleftrightarrow{\mathbf{M}}(\mathbf{k} = 0; \mathbf{G}, \mathbf{G}') = [(G^2 - k_0^2)\overleftrightarrow{\mathbf{I}} - \mathbf{GG}]\delta_{\mathbf{G},\mathbf{G}'} - \mathrm{i}\omega\mu_0\hat{\sigma}(\mathbf{G} - \mathbf{G}')\overleftrightarrow{\mathbf{I}}. \tag{42}$$

Note that $\overleftrightarrow{\boldsymbol{\Sigma}}^{(0)}$ can also be obtained from equation (25) by substituting $k = 0$. We obtain

$$\overleftrightarrow{\boldsymbol{\Sigma}}^{(0)} = \frac{\mathrm{i}}{\omega\mu_0}[\{\overleftrightarrow{\mathbf{N}}^{-1}(\mathbf{k} = 0; 0, 0)\}^{-1} + k_0^2\overleftrightarrow{\mathbf{I}}]. \tag{43}$$

As shown in appendix B, the linear term in the expansion equation (37) of $\overleftrightarrow{\boldsymbol{\Sigma}}(\mathbf{k})$ is

$$\overleftrightarrow{\boldsymbol{\Sigma}}^{(1)}(\hat{\mathbf{k}}) \equiv -\mathrm{i}\omega\mu_0 {\sum_{\mathbf{G}}}' \overleftrightarrow{\mathbf{C}}_1(\mathbf{G}) \cdot \overleftrightarrow{\mathbf{L}}(\hat{\mathbf{k}}, \mathbf{G}) \cdot \overleftrightarrow{\mathbf{C}}_2(\mathbf{G}), \tag{44}$$

$$\overleftrightarrow{\mathbf{L}}(\hat{\mathbf{k}}, \mathbf{G}) = 2(\hat{\mathbf{k}} \cdot \mathbf{G})\overleftrightarrow{\mathbf{I}} - (\hat{\mathbf{k}}\mathbf{G} + \mathbf{G}\hat{\mathbf{k}}), \tag{45}$$

$$\overleftrightarrow{\mathbf{C}}_2(\mathbf{G}) = {\sum_{\mathbf{G}'}}' \overleftrightarrow{\mathbf{M}}_0^{-1}(\mathbf{G}, \mathbf{G}')\hat{\sigma}(\mathbf{G}'). \tag{46}$$

The dyadic $\overleftrightarrow{\Sigma}^{(2)}(\hat{\mathbf{k}})$ in equation (37), also derived in appendix B, can be written as

$$\overleftrightarrow{\Sigma}^{(2)}(\hat{\mathbf{k}}) \equiv \mathrm{i}\omega\mu_0 \sum_{\mathbf{G},\mathbf{G}'}{}' \overleftrightarrow{C}_1(\mathbf{G}) \cdot [\overleftrightarrow{L}(\hat{\mathbf{k}}, \mathbf{G}) \cdot \overleftrightarrow{M}_0^{-1}(\mathbf{G}, \mathbf{G}') \cdot \overleftrightarrow{L}(\hat{\mathbf{k}}, \mathbf{G}') - (\overleftrightarrow{I} - \hat{\mathbf{k}}\hat{\mathbf{k}})\delta_{\mathbf{G},\mathbf{G}'}] \cdot \overleftrightarrow{C}_2(\mathbf{G}). \tag{47}$$

Next, it is convenient to rewrite the dyadics $\overleftrightarrow{\Sigma}^{(1)}$ and $\overleftrightarrow{\Sigma}^{(2)}$ formally as follows:

$$\overleftrightarrow{\Sigma}^{(1)} \equiv p\overleftrightarrow{I} \cdot \overleftrightarrow{\Sigma}^{(1)} + (1-p)\overleftrightarrow{\Sigma}^{(1)} \cdot \overleftrightarrow{I}, \tag{48}$$

$$\overleftrightarrow{\Sigma}^{(2)} \equiv \overleftrightarrow{I} \cdot \overleftrightarrow{\Sigma}^{(2)} \cdot \overleftrightarrow{I}. \tag{49}$$

Here, the artificially introduced fraction p can take, for the moment, any value. Its value will be determined below by imposing the Onsager symmetry relations [6, 64]. Employing the identities

$$\overleftrightarrow{I} = \hat{\mathbf{k}}\hat{\mathbf{k}} - \hat{\mathbf{k}} \times \hat{\mathbf{k}} \times \overleftrightarrow{I}, \tag{50}$$

and equation (48), together with Faraday's law (equation (28)), we can express $k\overleftrightarrow{\Sigma}^{(1)} \cdot \mathbf{E}$ as

$$k\overleftrightarrow{\Sigma}^{(1)} \cdot \mathbf{E} = p[\mathbf{k}\hat{\mathbf{k}} \cdot \overleftrightarrow{\Sigma}^{(1)} \cdot \mathbf{E} - \mathbf{k} \times \hat{\mathbf{k}} \times \overleftrightarrow{\Sigma}^{(1)} \cdot \mathbf{E}] + (1-p)[\overleftrightarrow{\Sigma}^{(1)} \cdot \hat{\mathbf{k}}\mathbf{k} \cdot \mathbf{E} - \omega\overleftrightarrow{\Sigma}^{(1)} \cdot \hat{\mathbf{k}} \times \mathbf{B}]. \tag{51}$$

In a similar way, $k^2\overleftrightarrow{\Sigma}^{(2)} \cdot \mathbf{E}$ can be transformed. We obtain

$$k^2\overleftrightarrow{\Sigma}^{(2)} \cdot \mathbf{E} = \mathbf{k}\hat{\mathbf{k}} \cdot \overleftrightarrow{\Sigma}^{(2)} \cdot \hat{\mathbf{k}}\mathbf{k} \cdot \mathbf{E} - \omega\mathbf{k}\hat{\mathbf{k}} \cdot \overleftrightarrow{\Sigma}^{(2)} \cdot \hat{\mathbf{k}} \times \mathbf{B} - \mathbf{k} \times \hat{\mathbf{k}} \times \overleftrightarrow{\Sigma}^{(2)} \cdot (\hat{\mathbf{k}}\mathbf{k} \cdot \mathbf{E} - \omega\hat{\mathbf{k}} \times \mathbf{B}). \tag{52}$$

Substituting equations (51) and (52) into equation (37) and this, in turn, into the Ampére–Maxwell law (equation (26)), and writing all the terms of $\overleftrightarrow{\Sigma}(\mathbf{k})$ that are of the form $\mathbf{k} \times \overleftrightarrow{\Lambda}(\mathbf{k})$ on the left-hand side, we obtain

$$\begin{aligned}\mathbf{k} \times \{\mathbf{B} - \mu_0\mathrm{i}\hat{\mathbf{k}} \times [p\overleftrightarrow{\Sigma}^{(1)} \cdot \mathbf{E} + \overleftrightarrow{\Sigma}^{(2)} \cdot \hat{\mathbf{k}}\mathbf{k} \cdot \mathbf{E} - \omega\overleftrightarrow{\Sigma}^{(2)} \cdot (\hat{\mathbf{k}} \times \mathbf{B}) + \cdots]\} \\ = -\omega\mu_0 \Big\{\varepsilon_0\mathbf{E} + \frac{\mathrm{i}}{\omega}[\overleftrightarrow{\Sigma}^{(0)} \cdot \mathbf{E} + p\mathbf{k}\hat{\mathbf{k}} \cdot \overleftrightarrow{\Sigma}^{(1)} \cdot \mathbf{E} + (1-p)\overleftrightarrow{\Sigma}^{(1)} \cdot \hat{\mathbf{k}}\mathbf{k} \cdot \mathbf{E} \\ + \mathbf{k}\hat{\mathbf{k}} \cdot \overleftrightarrow{\Sigma}^{(2)} \cdot \hat{\mathbf{k}}\mathbf{k} \cdot \mathbf{E} - (1-p)\omega\overleftrightarrow{\Sigma}^{(1)} \cdot (\hat{\mathbf{k}} \times \mathbf{B}) - \omega\mathbf{k}\hat{\mathbf{k}} \cdot \overleftrightarrow{\Sigma}^{(2)} \cdot (\hat{\mathbf{k}} \times \mathbf{B}) + \cdots]\Big\}.\end{aligned} \tag{53}$$

Comparing with equation (30), we can identify the expression in curly brackets on the left-hand side of this equation as the vector $\mu_0\mathbf{H}$:

$$\mu_0\mathbf{H} \equiv \mathbf{B} - \mu_0\mathrm{i}\hat{\mathbf{k}} \times [p\overleftrightarrow{\Sigma}^{(1)} \cdot \mathbf{E} + \overleftrightarrow{\Sigma}^{(2)} \cdot \hat{\mathbf{k}}\mathbf{k} \cdot \mathbf{E} - \omega\overleftrightarrow{\Sigma}^{(2)} \cdot (\hat{\mathbf{k}} \times \mathbf{B}) + \cdots]. \tag{54}$$

Comparison of equations (53) and (30) also identifies the displacement vector $\mathbf{D}$ as

$$\begin{aligned}\mathbf{D} \equiv \varepsilon_0\mathbf{E} + \frac{\mathrm{i}}{\omega}[\overleftrightarrow{\Sigma}^{(0)} \cdot \mathbf{E} + p\mathbf{k}\hat{\mathbf{k}} \cdot \overleftrightarrow{\Sigma}^{(1)} \cdot \mathbf{E} + (1-p)\overleftrightarrow{\Sigma}^{(1)} \cdot \hat{\mathbf{k}}\mathbf{k} \cdot \mathbf{E} + \mathbf{k}\hat{\mathbf{k}} \cdot \overleftrightarrow{\Sigma}^{(2)} \cdot \hat{\mathbf{k}}\mathbf{k} \cdot \mathbf{E} \\ - (1-p)\omega\overleftrightarrow{\Sigma}^{(1)} \cdot (\hat{\mathbf{k}} \times \mathbf{B}) - \omega\mathbf{k}\hat{\mathbf{k}} \cdot \overleftrightarrow{\Sigma}^{(2)} \cdot (\hat{\mathbf{k}} \times \mathbf{B}) + \cdots].\end{aligned} \tag{55}$$

Due to our assumption (equation (10)), it is of particular interest to determine the material equations in the limit $k \to 0$. The resulting expressions for $\mathbf{D}$ and $\mathbf{H}$ in this limit are

$$\mathbf{D} \equiv \varepsilon_0\mathbf{E} + \frac{\mathrm{i}}{\omega}[\overleftrightarrow{\Sigma}^{(0)} \cdot \mathbf{E} - (1-p)\omega\overleftrightarrow{\Sigma}^{(1)} \cdot (\hat{\mathbf{k}} \times \mathbf{B})], \tag{56}$$

$$\mu_0\mathbf{H} \equiv \mathbf{B} - \mu_0\mathrm{i}\hat{\mathbf{k}} \times [p\overleftrightarrow{\Sigma}^{(1)} \cdot \mathbf{E} - \omega\overleftrightarrow{\Sigma}^{(2)} \cdot (\hat{\mathbf{k}} \times \mathbf{B})]. \tag{57}$$

Note that in equations (56) and (57) the terms proportional to ω have been kept because for optical bands they can be of the same order as the first terms. These expressions can be rewritten in the form of the *magneto-dielectric* response

$$\mathbf{D} = \overleftrightarrow{\boldsymbol{\alpha}} \cdot \mathbf{E} + \overleftrightarrow{\boldsymbol{\beta}} \cdot \mathbf{B}, \quad \mathbf{H} = \overleftrightarrow{\boldsymbol{\phi}} \cdot \mathbf{E} + \overleftrightarrow{\boldsymbol{\psi}} \cdot \mathbf{B}, \tag{58}$$

$$\overleftrightarrow{\boldsymbol{\alpha}} = \varepsilon_0 \overleftrightarrow{\mathbf{I}} + (\mathrm{i}/\omega) \overleftrightarrow{\boldsymbol{\Sigma}}^{(0)}, \tag{59}$$

$$\overleftrightarrow{\boldsymbol{\beta}} = -\mathrm{i}(1-p) \overleftrightarrow{\boldsymbol{\Sigma}}^{(1)}(\hat{\mathbf{k}}) \cdot (\hat{\mathbf{k}} \times \overleftrightarrow{\mathbf{I}}), \tag{60}$$

$$\overleftrightarrow{\boldsymbol{\phi}} = -\mathrm{i}p \hat{\mathbf{k}} \times \overleftrightarrow{\boldsymbol{\Sigma}}^{(1)}(\hat{\mathbf{k}}), \tag{61}$$

$$\overleftrightarrow{\boldsymbol{\psi}} = (1/\mu_0) \overleftrightarrow{\mathbf{I}} + \mathrm{i}\omega \hat{\mathbf{k}} \times \overleftrightarrow{\boldsymbol{\Sigma}}^{(2)}(\hat{\mathbf{k}}) \cdot (\hat{\mathbf{k}} \times \overleftrightarrow{\mathbf{I}}). \tag{62}$$

Comparing the magneto-electric response (equation (58)) with the conventional bianisotropic response (equations (38) and (39)), it is straightforward to establish the relations, also derived in [25],

$$\overleftrightarrow{\boldsymbol{\varepsilon}} = \overleftrightarrow{\boldsymbol{\alpha}} - \overleftrightarrow{\boldsymbol{\beta}} \cdot \overleftrightarrow{\boldsymbol{\psi}}^{-1} \cdot \overleftrightarrow{\boldsymbol{\phi}}, \quad \overleftrightarrow{\boldsymbol{\gamma}} = \overleftrightarrow{\boldsymbol{\beta}} \cdot \overleftrightarrow{\boldsymbol{\psi}}^{-1}, \quad \overleftrightarrow{\boldsymbol{\delta}} = -\overleftrightarrow{\boldsymbol{\psi}}^{-1} \cdot \overleftrightarrow{\boldsymbol{\phi}}, \quad \overleftrightarrow{\boldsymbol{\mu}} = \overleftrightarrow{\boldsymbol{\psi}}^{-1}. \tag{63}$$

The artificially introduced parameter p is determined by imposing the Onsager symmetry relations [6, 64]

$$\overleftrightarrow{\boldsymbol{\varepsilon}} = \overleftrightarrow{\boldsymbol{\varepsilon}}_{\mathrm{T}}, \quad \overleftrightarrow{\boldsymbol{\mu}} = \overleftrightarrow{\boldsymbol{\mu}}_{\mathrm{T}}, \quad \overleftrightarrow{\boldsymbol{\delta}} = -\overleftrightarrow{\boldsymbol{\gamma}}_{\mathrm{T}}, \tag{64}$$

where the subscripts T denote transpositions of the dyadics. It is shown in appendix C that these relations between the effective dyadics of the bianisotropic response are satisfied only for $p = 1/2$.

It is interesting to note that the effective dyadics $\overleftrightarrow{\boldsymbol{\varepsilon}}$, $\overleftrightarrow{\boldsymbol{\gamma}}$ and $\overleftrightarrow{\boldsymbol{\mu}}$ depend on the *direction* of the wave vector $\mathbf{k}$, which introduces anisotropy additional to that of the lattice. It means that, in general, these dyadics diagonalize in different coordinate systems. This must have important consequences for the response at the macro-level. Nevertheless, the dyadics defining the bianisotropic response (as well as those of the magneto-dielectric response) are independent of the *magnitude* of the wave vector $\mathbf{k}$. On the other hand, as we have seen in section 3, the dielectric response, *to the same physical precision*, incorporates terms in $\overleftrightarrow{\boldsymbol{\varepsilon}}(\mathbf{k}, \omega)$ that are linear and quadratic in $\mathbf{k}$.

Now we are in a position to derive the wave equation for the electric field in terms of the dyadics that describe the effective medium.

5. Dispersion relation of the homogenized medium

The dispersion relation for the electromagnetic modes in the homogenized medium can be obtained by substituting the bianisotropic response (equation (58)) into the macroscopic Maxwell equations (equations (30)–(33)). Solving for the macroscopic electric field $\mathbf{E}$, we obtain

$$[\omega^2 \overleftrightarrow{\boldsymbol{\alpha}} + \omega\, \mathbf{k} \times \overleftrightarrow{\boldsymbol{\phi}}(\hat{\mathbf{k}}) + (\omega\, \overleftrightarrow{\boldsymbol{\beta}}(\hat{\mathbf{k}}) + \mathbf{k} \times \overleftrightarrow{\boldsymbol{\psi}}(\hat{\mathbf{k}})) \cdot (\mathbf{k} \times \overleftrightarrow{\mathbf{I}})] \cdot \mathbf{E} = 0. \tag{65}$$

Even though the material dyadics are complicated functions of ω and $\hat{\mathbf{k}}$, it is, in principle, possible to solve equation (65) for any given ω or $\mathbf{k}$. It is important to note that, *for transverse*

modes, substitution of equations (59)–(62) into (65) is equivalent to the band structure problem in the limit $\mathbf{k} \to 0$; on the other hand, this substitution may not always yield *longitudinal modes* with sufficient precision. The use of equation (65) can result in an important simplification for high-symmetry systems. In such cases, it is possible to calculate the effective permeability from the band structure and the effective permittivity, rather than using the direct procedure, namely, the substitution of equation (62) into the last equation of (63). The evaluation of $\overleftrightarrow{\boldsymbol{\Sigma}}^{(2)}$ is thus avoided and computation time is saved.

6. Analytic results for special cases

In this section, we will analyze the bianisotropic response in several important cases, considering first generalities (section 6.1) and later specific systems (section 6.2).

6.1. Generalities

6.1.1. Inversion symmetry. If the unit cell of the homogenized PC is composed of inclusions possessing inversion symmetry, then $\overleftrightarrow{\boldsymbol{\Sigma}}(-\mathbf{k}) = \overleftrightarrow{\boldsymbol{\Sigma}}(\mathbf{k})$. Hence, it follows from equation (37) that

$$\overleftrightarrow{\boldsymbol{\Sigma}}^{(1)}(\hat{\mathbf{k}}) = 0. \tag{66}$$

Hence, by equations (60) and (61), as well as $\overleftrightarrow{\boldsymbol{\beta}} = \overleftrightarrow{\boldsymbol{\phi}} = 0$, and using equation (63), the conventional bianisotropic response acquires the form

$$\begin{aligned} &\mathbf{D} = \overleftrightarrow{\boldsymbol{\varepsilon}} \cdot \mathbf{E}, && \overleftrightarrow{\boldsymbol{\varepsilon}} = \varepsilon_0 \overleftrightarrow{\mathbf{I}} + (\mathrm{i}/\omega)\overleftrightarrow{\boldsymbol{\Sigma}}^{(0)}, \\ &\mathbf{B} = \overleftrightarrow{\boldsymbol{\mu}}(\hat{\mathbf{k}}) \cdot \mathbf{H}, && \overleftrightarrow{\boldsymbol{\mu}}^{-1}(\hat{\mathbf{k}}) = (1/\mu_0)\,\overleftrightarrow{\mathbf{I}} + \mathrm{i}\omega\hat{\mathbf{k}} \times \overleftrightarrow{\boldsymbol{\Sigma}}^{(2)}(\hat{\mathbf{k}}) \cdot (\hat{\mathbf{k}} \times \overleftrightarrow{\mathbf{I}}). \end{aligned} \tag{67}$$

Here, we can see that the permittivity tensor $\overleftrightarrow{\boldsymbol{\varepsilon}}$, being independent of the unit vector $\hat{\mathbf{k}}$, must be diagonal in some coordinate system that is embedded in the PC. On the other hand, the permeability dyadic $\overleftrightarrow{\boldsymbol{\mu}}(\hat{\mathbf{k}})$ diagonalizes in a coordinate system that has one axis parallel to $\hat{\mathbf{k}}$. This is seen from the fact that, for any unit vector $\hat{\mathbf{l}} \perp \hat{\mathbf{k}}$, the following off-diagonal matrix elements vanish:

$$(\overleftrightarrow{\boldsymbol{\mu}}^{-1})_{\hat{\mathbf{k}}\hat{\mathbf{l}}} = (\overleftrightarrow{\boldsymbol{\mu}}^{-1})_{\hat{\mathbf{l}}\hat{\mathbf{k}}} = 0, \tag{68}$$

as follows from the last equation of (67). As for the corresponding diagonal element,

$$(\overleftrightarrow{\boldsymbol{\mu}}^{-1})_{\hat{\mathbf{k}}\hat{\mathbf{k}}} = \hat{\mathbf{k}} \cdot \overleftrightarrow{\boldsymbol{\mu}}^{-1}(\hat{\mathbf{k}}) \cdot \hat{\mathbf{k}} = (1/\mu_0). \tag{69}$$

However, this element has no repercussions because equation (30) gives the same result as when it is omitted. The reason for the element $(\overleftrightarrow{\mu}^{-1})_{\hat{\mathbf{k}}\hat{\mathbf{k}}}$ having no physical relevance is that the Maxwell law (equation (30)) has nothing to say about a component of $\mathbf{H}$ parallel to $\mathbf{k}$, and such a component cannot exist. In fact, this is even true in the absence of inversion symmetry and is a result of the nonexistence of magnetic charges, $\nabla \cdot \mathbf{B} = 0$. (Indeed, it follows from equation (54) that $\mathbf{H} \cdot \hat{\mathbf{k}} = \mathbf{B} \cdot \hat{\mathbf{k}} = 0$.)

In a system possessing inversion symmetry, the general dispersion relation (equation (65)) simplifies to

$$\omega^2 \overleftrightarrow{\boldsymbol{\varepsilon}} \cdot \mathbf{E} + \mathbf{k} \times \overleftrightarrow{\boldsymbol{\mu}}^{-1}(\hat{\mathbf{k}}) \cdot (\mathbf{k} \times \mathbf{E}) = 0. \tag{70}$$

This result has been derived previously by Amirkhizi and Nemat-Nasser [65].

6.1.2. Cubic symmetry. Now, let us consider the case of cubic symmetry, according to which the permittivity and permeability tensors have the form

$$\overleftrightarrow{\boldsymbol{\varepsilon}} = \varepsilon \overleftrightarrow{\mathbf{I}}, \tag{71}$$

$$\overleftrightarrow{\boldsymbol{\mu}}^{-1}(\hat{\mathbf{k}}) = (1/\mu_0)\hat{\mathbf{k}}\hat{\mathbf{k}} + (1/\mu)(\overleftrightarrow{\mathbf{I}} - \hat{\mathbf{k}}\hat{\mathbf{k}}). \tag{72}$$

The first term of equation (72) follows from equation (69). However, because this term does not contribute (as pointed out after equation (69)), in practice we can replace μ_0 by μ and write simply

$$\mathbf{D} = \varepsilon \mathbf{E}, \quad \mathbf{B} = \mu \mathbf{H}. \tag{73}$$

Hence, for the cubic symmetry the material response is isotropic. Obviously, the dispersion relation for the electromagnetic waves in the homogenized material is given by

$$k^2 = \omega^2 \varepsilon \mu. \tag{74}$$

We should note that the diagonal form of the permittivity and permeability tensors (equations (71) and (72)) follows from the explicit analytic expressions for the tensors of the effective bianisotropic response (equations (40), (47) and (67)), which depend on PC symmetry. However, it should be noted that in calculating the effective tensors with our derived formulae, the direction of the wave vector ($\mathbf{k} \to 0$) has to be specified. We could analytically verify the diagonal form of the permittivity and permeability tensors for the cubic symmetry by assuming that the wave vector ($\mathbf{k} \to 0$) is parallel to one of the principal axes of the photonic crystal. The diagonal form of these tensors for cubic symmetry and arbitrary choice of the wave vector ($\mathbf{k} \to 0$) can be verified only by numerical calculations.

6.1.3. Mutually perpendicular mirror planes (two-dimensional (2D) photonic crystal). Consider a 2D PC of cylinders parallel to the z-axis and possessing mirror planes perpendicular to the x- and y-axes. Such a structure has inversion symmetry (equation (66)) and also satisfies the following equation:

$$\hat{\sigma}(-\mathbf{G}_x, \mathbf{G}_y) = \hat{\sigma}(\mathbf{G}_x, \mathbf{G}_y) = \hat{\sigma}(\mathbf{G}_x, -\mathbf{G}_y). \tag{75}$$

As a consequence of equation (75), $\overleftrightarrow{\boldsymbol{\varepsilon}}$ is always a diagonal tensor in the natural PC coordinate system ($\hat{\mathbf{x}}$, $\hat{\mathbf{y}}$, $\hat{\mathbf{z}}$). Again, $\overleftrightarrow{\boldsymbol{\mu}}(\hat{\mathbf{k}})$ can be diagonal only in a reference system ($\hat{\mathbf{k}}$, $\hat{\mathbf{l}}$, $\hat{\mathbf{m}}$) in which one of the axes is parallel to $\hat{\mathbf{k}}$. Of course, when an electromagnetic wave propagates in a high-symmetry direction, both dyadics $\overleftrightarrow{\boldsymbol{\varepsilon}}$ and $\overleftrightarrow{\boldsymbol{\mu}}$ are diagonal.

For example, consider an electromagnetic wave propagating in the $\hat{\mathbf{x}}$ direction, i.e. $\hat{\mathbf{k}} = \hat{\mathbf{x}}$. Equations (59) and (62) result in diagonal tensors and, because of the mirror planes considered (equivalent to a fourfold rotation axis z), $\varepsilon_{xx} = \varepsilon_{yy} \equiv \varepsilon_\perp$, $\mu_{xx} = \mu_{yy} \equiv \mu_\perp$, $\varepsilon_{zz} \equiv \varepsilon_\parallel$, $\mu_{zz} \equiv \mu_\parallel$; in dyadic notation

$$\overleftrightarrow{\boldsymbol{\varepsilon}} = \varepsilon_\perp(\hat{\mathbf{x}}\hat{\mathbf{x}} + \hat{\mathbf{y}}\hat{\mathbf{y}}) + \varepsilon_\parallel \hat{\mathbf{z}}\hat{\mathbf{z}}, \tag{76}$$

$$\overleftrightarrow{\boldsymbol{\mu}} = \mu_\perp(\hat{\mathbf{x}}\hat{\mathbf{x}} + \hat{\mathbf{y}}\hat{\mathbf{y}}) + \mu_\parallel \hat{\mathbf{z}}\hat{\mathbf{z}}. \tag{77}$$

Substituting equations (76) and (77) into (70), we find two possible solutions, as expected, one for the E-mode (with the electric field in the $\hat{\mathbf{z}}$ direction) and the other for the H-mode (with the magnetic field in the $\hat{\mathbf{z}}$ direction),

$$k_x^2 = \omega^2 \varepsilon_\parallel \mu_\perp \quad \text{E-mode}, \tag{78}$$

$$k_x^2 = \omega^2 \varepsilon_\perp \mu_\parallel \quad \text{H-mode.} \tag{79}$$

From equations (78) and (79), we conclude that it is always possible to obtain the effective permeability from the dispersion relation $\omega(k)$ when the effective permittivity is known for high-symmetry conditions. This can result in considerable saving of computing time. Similar conclusions are obtained for high-symmetry 3Ds (see equation (74)) and for 1D PCs. Nevertheless, in exceptional cases the computation of ε can be more problematic than the determination of μ. In such situations equations (78) and (79) can be used to find ε as, in fact, we did for the H-mode of metallic cylinders; see section 7.3.

6.2. *Specific systems*

6.2.1. Small spheres in a cubic lattice. We have applied equation (67) to calculate the effective ε and μ of a cubic PC with a small sphere of radius r in every unit cell. Hence, the filling fraction f is assumed to be very small:

$$f = \frac{4\pi}{3}\frac{r^3}{a^3} \ll 1, \tag{80}$$

with a being the lattice constant. The generalized conductivities for the spherical inclusion and the host material are, respectively, $\hat{\sigma}_a$ and $\hat{\sigma}_b$. Because of the cubic symmetry, $\overleftrightarrow{\boldsymbol{\Sigma}}^{(0)}$, as given by equation (43), must be proportional to the unit dyadic $\overleftrightarrow{\mathbf{I}}$. Hence, equation (67) reduces to the scalar response (equation (73)). In obtaining ε, we have calculated the dyadic $\overleftrightarrow{\mathbf{N}}^{-1}(\mathbf{k} = 0; 0, 0)$ assuming that $r \ll a$. Details of this approximate calculation of the dyadic $\overleftrightarrow{\mathbf{N}}^{-1}(\mathbf{k} = 0; 0, 0)$ are explained in appendix D. We obtain

$$\overleftrightarrow{\mathbf{N}}^{-1}(\mathbf{k} = 0; 0, 0) = \frac{1}{k_0^2 + \mathrm{i}\omega\mu_0\hat{\sigma}_b}\left(\frac{\mathrm{i}\omega\mu_0\left(\hat{\sigma}_a - \hat{\sigma}_b\right) f}{k_0^2 + \mathrm{i}\omega\mu_0\left[\left(\hat{\sigma}_a - \hat{\sigma}_b\right)\left(\frac{2}{3}f + \frac{1}{3}\right) + \hat{\sigma}_b\right]} - 1\right)\overleftrightarrow{\mathbf{I}}. \tag{81}$$

After some algebraic operations and using equations (43) and (67), we find that

$$\varepsilon = \varepsilon_b \frac{1 + 2f\frac{\varepsilon_a - \varepsilon_b}{\varepsilon_a + 2\varepsilon_b}}{1 - f\frac{\varepsilon_a - \varepsilon_b}{\varepsilon_a + 2\varepsilon_b}}, \tag{82}$$

where

$$\varepsilon_a = \varepsilon_0 + \mathrm{i}\hat{\sigma}_a/\omega, \quad \varepsilon_b = \varepsilon_0 + \mathrm{i}\hat{\sigma}_b/\omega. \tag{83}$$

This result for ε coincides with the well-known Maxwell–Garnett formula for the effective dielectric constant of a composite. In this case, $\mu \approx \mu_0$.

6.2.2. Cubic lattice of metallic wires. We have also applied our results to another cubic photonic crystal, which is constructed with thin metallic wires ('3D crosses'). Here, the dyadic $\overleftrightarrow{\mathbf{N}}^{-1}(\mathbf{k} = 0; \mathbf{G}, \mathbf{G}')$ and, consequently, the permittivity ε (equation (67)) were calculated approximately by assuming that the radius of the wires r_0 is much smaller than the lattice constant a. The final result for the dielectric constant is (see appendix E)

$$\frac{\varepsilon(\omega)}{\varepsilon_0} = 1 - \frac{\omega_0^2}{\omega(\omega + \mathrm{i}\rho\omega_0^2)}, \qquad \omega_0^2 = \frac{2\pi c^2}{a^2 \ln(a/r_0)}, \qquad \rho = \frac{\varepsilon_0 a^2}{\pi r_0^2 \sigma}, \tag{84}$$

where σ is the usual conductivity of the metal. This is in agreement with Pendry *et al*'s plasma model [23] with effective plasma frequency ω_0 and damping frequency $\rho\omega_0^2$. A similar expression for the effective permittivity is obtained for wires with square cross-section, but with ω_0^2 and ρ given by (see appendix E)

$$\omega_0^2 = \frac{2\pi c^2}{a^2 \ln(a/l)}, \qquad \rho = \frac{\varepsilon_0 a^2}{l^2 \sigma}, \tag{85}$$

where l is the side length of the square cross-section. For this kind of structure, $\mu \approx \mu_0$.

7. Numerical results

The effective parameters ε and μ can be calculated analytically only for a few high-symmetry structures, as was shown in the previous section for a cubic array of spheres and wires. In general, the response at the macro-level must be obtained numerically. In this section, we present computational results for the effective permittivity and permeability of several well-known photonic structures. As a check, we have also compared our results with other homogenization theories reported in the literature.

7.1. 2D dielectric cylinders

As a first check, we have obtained the effective parameters of a 2D PC formed by circular dielectric cylinders in a square lattice. Strictly speaking, the quasi-static limit is studied, although in practice the results hold up to frequencies as high as about the middle of the first (acoustic) band, with quite good precision. Two complementary cases are presented, namely silicon cylinders in an air host and air cylinders in a silicon host. Figure 1 shows the effective permittivity and permeability as a function of the filling fraction. Such a structure presents isotropy in the plane of periodicity, resulting in a uni-axial dyadic for the effective permittivity, namely equation (76):

$$\overleftrightarrow{\boldsymbol{\varepsilon}} = \begin{Bmatrix} \varepsilon_\perp & 0 & 0 \\ 0 & \varepsilon_\perp & 0 \\ 0 & 0 & \varepsilon_\parallel \end{Bmatrix}. \tag{86}$$

The solid line corresponds to the solution of equation (67) for $\overleftrightarrow{\boldsymbol{\varepsilon}}$ and the dashed line to the results obtained for the same structure in [10]. The calculations show good agreement, except for the $\varepsilon_\parallel$ component in the region of very high filling fractions. As expected, because of the simplicity of the system, these dielectric structures do not present resonances and there are no magnetic effects. Our method gives the correct answer, with $\overleftrightarrow{\boldsymbol{\mu}} = \mu_0 \overleftrightarrow{\mathbf{I}}$ for any filling fraction. It is important to stress that the method presented in [10] assumes that there are no magnetic effects ($\mu = \mu_0$ for any ω) and is valid only for dielectric structures in the region where the dispersion relation $\omega(k)$ is linear.

7.2. 3D dielectric spheres

Figure 2 shows the effective permittivity and permeability for a 3D PC composed of silicon spheres in an air host for different values of the filling fraction. As in section 7.1, the quasi-static limit has been considered. Owing to the cubic symmetry of the system, the electromagnetic

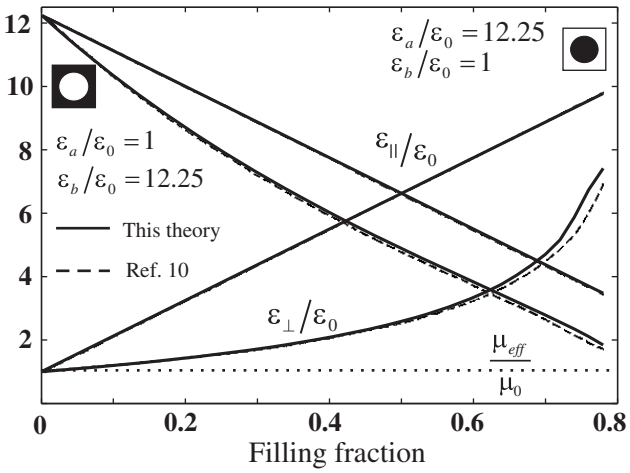

Figure 1. Effective permittivity and permeability of arrays of circular Si rods in air and of cylindrical holes in a Si host as a function of the filling fraction. The subindex a (b) refers to the cylindrical inclusions (host medium surrounding the inclusions). Solid lines correspond to the principal dielectric constants and dotted lines to the effective permeability. In this case, we used 1517 **G** values in the computation. For these simple dielectric structures there are no magnetic effects, as expected. Dashed lines correspond to the results obtained for the same structure in [10]. There is good agreement between the calculations, especially for $f < 0.6$.

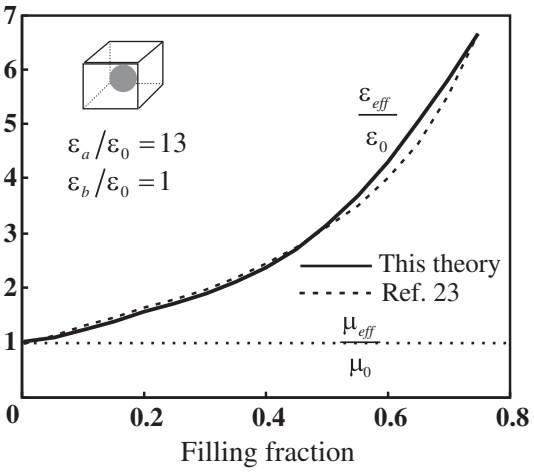

Figure 2. Effective permittivity (solid line) and effective permeability (dotted line) of a 3D PC of dielectric spheres in a cubic lattice as a function of the filling fraction. In this case, we used 1793 **G** values in the computation, resulting in very good convergence. As in figure 1, there are no magnetic effects. Dashed lines correspond to the effective permittivity obtained in [31] for the same structure. There is good agreement between the calculations except for the region around $f \approx 0.64$.

properties can be completely defined in terms of two scalars, ε and μ; see equations (71)–(73). The solid line corresponds to the effective permittivity computed using equation (67) and the dashed line describes the effective permittivity calculated by Datta *et al* [31] for the same system. There is good agreement, especially for small filling fractions. Again, for this simple dielectric structure with $\omega \propto k$, $\mu = \mu_0$ for any filling fraction.

7.3. 2D metallic wires

A bidimensional metallo-dielectric PC of metallic wires has two different types of behavior, depending on the polarization of the incident wave. For the E-mode (with the electric field parallel to the wires) the structure presents a low-frequency band gap [66]. This behavior is correctly described by the effective parameters obtained from equation (67). Figure 3 presents the dispersion relation $\omega(k_x)$ for the first band and the relevant elements of the effective permittivity and permeability dyadics for a square lattice of copper wires ($\omega_p = 6.0774 \times 10^{15}\ s^{-1}$), considering three different filling fractions. We have fixed the wave propagation to the [100] direction. Figure 3(a) shows how the low-frequency band gap becomes wider as the filling fraction is increased. At the same time the first band is raised in frequency, while its width decreases. Figure 3(b) shows the effective permittivity $\varepsilon_\parallel$ and the effective permeability $\mu_\perp$ as a function of the frequency. We should note that inside the band gap $\varepsilon_\parallel$ and $\mu_\perp$ always have opposite signs, namely $\varepsilon < 0$ and $\mu \geqslant \mu_0$. This results in an imaginary effective refractive index, as corresponds to prohibition of propagation in this frequency range. When the frequency is increased, $\varepsilon_\parallel$ goes from negative to positive values, being equal to zero at the upper edge of the band gap. On the other hand, $\mu_\perp$ is strictly equal to μ_0 for $\omega = 0$ as follows from equation (67). When the frequency is increased, $\mu_\perp$ acquires values greater than μ_0, resulting in paramagnetic behavior.

Another situation is observed for the same structure of metallic wires when the electric field of the incident wave is in the plane of periodicity. For this polarization (H-mode), there is no low-frequency band gap and the dispersion $\omega(k_x)$ is linear at low frequencies. Nevertheless, as was pointed out by Krokhin *et al* [33] for the H-mode, this structure composed of nonmagnetic materials shows remarkable diamagnetic behavior. Figure 4 shows the effective permeability $\mu_\parallel$ (panel (a)) and the corresponding effective permittivity $\varepsilon_\perp$ (panel (b)) as a function of the filling fraction in the limit $k \to 0$ (and $\omega \to 0$) for three different metals, namely aluminum, copper and bismuth (with plasma frequencies $\omega_p = 2.278 \times 10^{16}\ s^{-1}$, $6.077 \times 10^{15}\ s^{-1}$ and $9.844 \times 10^{12}\ s^{-1}$, respectively). In panel (a), the solid lines were obtained from equation (67) and the dotted lines are the results obtained in [33]. As before, we get good agreement between the two methods, with the exception of high filling fractions where we do not reach convergence (dashed lines) with the 1405 'plane waves' used in this computation. The agreement in this region can be improved by increasing the number of plane waves. This behavior is also observed in dielectric structures, where small filling fractions require a smaller number of 'plane waves' in order to obtain convergence in the computation. Using figure 4(a) for the permeability, the effective permittivity $\varepsilon_\perp$, figure 4(b), was obtained with the help of equation (79). We note that direct computation of the permittivity from equation (67) ran into convergence problems while, in this particular situation, it was quite easy to obtain good convergence for the permeability.

7.4. 3D crosses of continuous and cut wires

We have calculated the effective permittivity and the effective permeability of a 3D metallo-dielectric PC of thin metallic wires of square cross-section (l^2) in a cubic lattice. Three cases

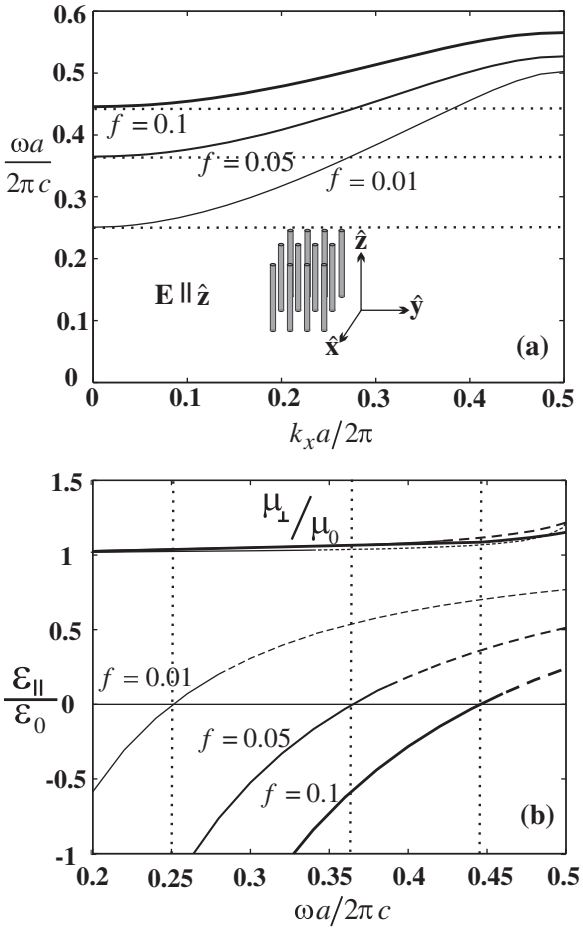

Figure 3. E-mode dispersion relation $\omega(k_x)$ for the first band (a) and the relevant elements of the effective permittivity and permeability dyadics (b) for a square lattice of copper wires ($\omega_p^{Cu} = 6.077 \times 10^{15}\,s^{-1}$) with a lattice constant $a = 1.5 \times 10^{-4}$ cm. Three different filling fractions are considered. We have fixed the wave propagation along the [100] direction and we have used 1405 **G** values in the computation. The system presents a low-frequency band gap in which the effective refractive index is imaginary. In addition, the system also presents paramagnetic behavior inside the first pass-band. The dotted lines mark the lower edges of the pass-bands. The dashed lines indicate regions ($k_x > \pi/2a$) where our long-wavelength expansion cannot be trusted.

are presented: crosses of continuous wires (figure 5(a)), crosses of cut wires separated by a small gap of width $d = 0.001\,05a$ (figure 6(a)) and crosses of cut wires with a larger gap $d = 0.002\,62a$ (figure 7(a)). The wires are characterized by a very high conductivity given by $\sigma = 10^7/a\mu_0 c$. Note that it is not necessary to specify the lattice constant a; it serves as a normalization constant. As before, because of the cubic symmetry of the system the electromagnetic properties are completely defined by two scalars, ε and μ. These effective parameters were calculated by using equations (67), (25) and $\overleftrightarrow{\Sigma}^{(2)} = \lim_{k\to 0}(\overleftrightarrow{\Sigma}(k) - \overleftrightarrow{\Sigma}^{(0)})/k^2$. In the calculation of the matrix block $\overleftrightarrow{N}^{-1}(\mathbf{k}; 0, 0)$, appearing in equation (25), we have taken advantage of the square cross-section by dividing the wires into a set of n small cubes of side l

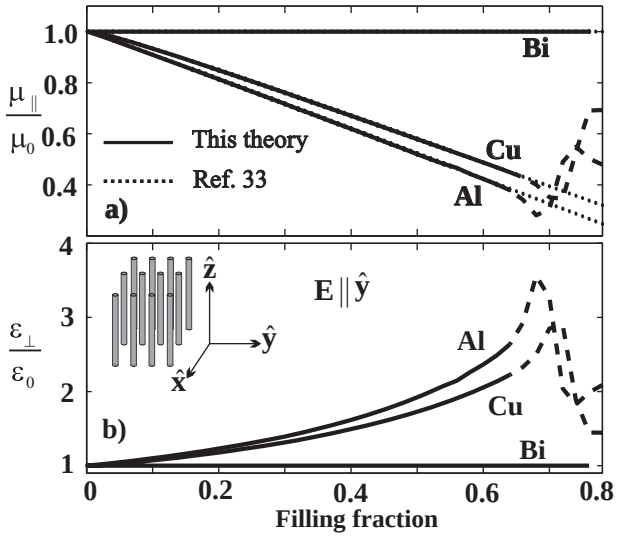

Figure 4. Effective permeability $\mu_\parallel$ (a) and effective permittivity $\varepsilon_\perp$ (b) for the H-mode as a function of the filling fraction in the limit $k \to 0$ (and $\omega \to 0$) for a square lattice of metallic wires with a lattice constant $a = 1.5 \times 10^{-4}$ cm. Three different metals are considered: aluminum ($\omega_p^{Al} = 2.278 \times 10^{16}\,s^{-1}$), copper ($\omega_p^{Cu} = 6.077 \times 10^{15}\,s^{-1}$) and bismuth ($\omega_p^{Bi} = 9.844 \times 10^{12}\,s^{-1}$). In panel (a), the solid lines were obtained from equation (67) and the dotted lines are the results obtained in [33]. The two methods show good agreement, with the exception of high filling fractions where we do not reach convergence (dotted lines) with the 1405 **G** values used in this computation. The diamagnetic behavior observed for copper and aluminum increases with the filling fraction. The effective permittivity $\varepsilon_\perp$ (b) was obtained from panel (a) and the dispersion relation $\omega(k_x)$.

and using the approach of small inclusions (see appendix D, equation (D.10)) for the form factor of each cube. This numerical method, known as the form-factor division approach [60], has led to an algebraic system of $3n$ equations. In our calculations, we used 55 small cubes (i.e. $n = 55$) and the results converged when the summations over **G** in the $3n \times 3n$ coefficients of this system had $N = (61)^3$ summands (where $N = 226\,981$ also denotes the number of 'plane waves'). The form-factor division approach is particularly useful when the filling fraction f of the inclusions is small because n should not be very large. Figures 5–7 are organized as follows: panel (a) gives the geometry of the system, where we have drawn two neighboring unit cells, zooming in on the interface region. In panel (b) is shown the effective permittivity ε of the structure, with its real part ε' plotted with solid lines and the imaginary part ε'' with dotted lines. The effective permeability is rendered in panel (c), again with solid (dotted) lines for the real (imaginary) part μ' (μ''). In panel (d), we have plotted the corresponding effective refractive index $n = \pm[(\varepsilon/\varepsilon_0)(\mu/\mu_0)]^{1/2}$ calculated from panels (b) and (c), with a similar convention for the real (n') and imaginary (n'') parts. Finally, in panel (e) we show the dispersion relation obtained from the effective parameters ε and μ. The same types of lines are used for the real (k') and imaginary (k'') wave vector components. Note that we have used dashed lines in the region $|\mathbf{k}| > \pi/2a$ where the quantitative description given by our homogenization theory is suspect. Nevertheless, the description is still expected to be useful qualitatively. In figure 8, we summarize the general behavior of this structure.

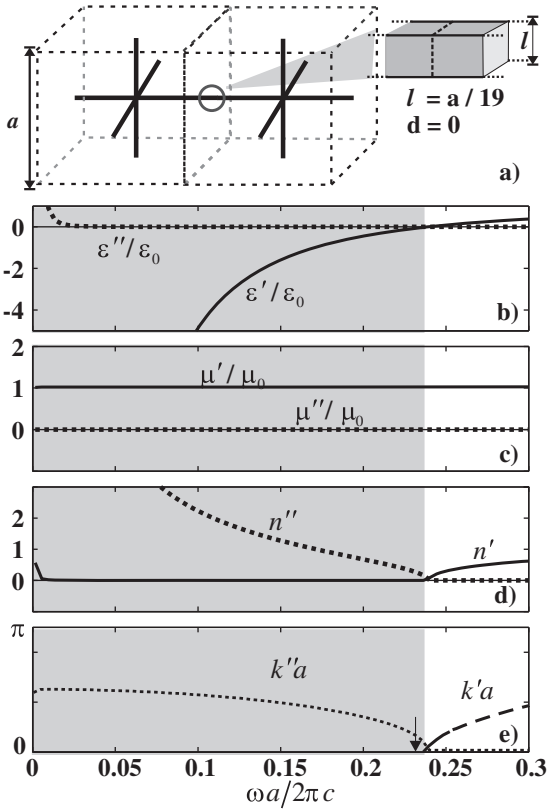

Figure 5. Effective parameters of a cubic lattice of continuous metallic wires (3D crosses) of square cross-section (chosen for computational convenience). The system is depicted in panel (a) where we have zoomed in on the interface region between two neighboring unit cells. The effective permittivity and permeability are plotted in panels (b) and (c), respectively. The corresponding effective refractive index is presented in panel (d). The dispersion relation $\omega(k)$, calculated from ε and μ, is plotted in panel (e), where the arrow indicates the effective plasma frequency obtained from equation (85). Shaded regions indicate the PBG, where n is imaginary. The system presents plasma-like behavior.

As was pointed out by Pendry *et al* [24], the electromagnetic behavior of this kind of structure strongly depends on the connectivity of the wires. For the case of continuous wires (figure 5), the system presents plasma-like behavior and a low-frequency band gap occurs (panel (e)). Inside this band gap region (shaded zones) the effective parameters ε and μ have opposite signs, namely $\varepsilon < 0$ and $\mu \geqslant 1$, and the corresponding effective refractive index n is imaginary. The arrow in panel (e) indicates the effective plasma frequency obtained from equation (85). The difference between equation (85) and our numerical result decreases as the wires become thinner. This is because equation (85) was derived assuming very thin wires. We note that the system of connected metallic wires has been recently investigated by Silveirinha, employing the homogenization method of [67].

When the thin wires are severed, the plasma-like behavior disappears and free-photon-like behavior emerges (figure 6). Now, low-frequency propagation of transverse modes is allowed as is shown in figure 6(e). It is important to note that this cut in the wires also creates a

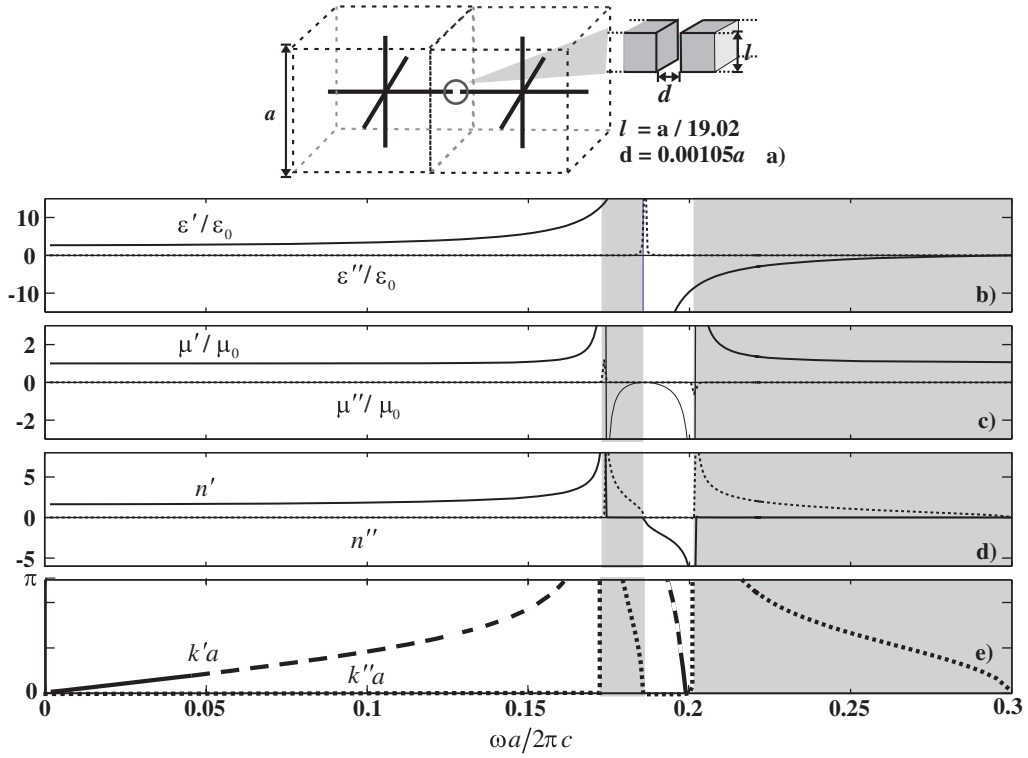

Figure 6. Effective parameters for a PC composed of 3D metallic crosses separated by a small gap. The system is depicted in panel (a) where we have zoomed in on the interface region between two neighboring unit cells. The effective permittivity and permeability are plotted in panels (b) and (c), respectively. The corresponding effective refractive index is presented in panel (d). The dispersion relation $\omega(k)$ calculated from ε and μ is plotted in panel (e). Shaded regions describe photonic band gaps where n is imaginary or complex. The first (acoustic) pass-band is characterized by a real and positive n, whereas the second (optical) band is characterized by a real and negative n. Long dashed lines indicate large k values for which our calculations in the limit $k \to 0$ cannot be trusted.

resonance and an anti-resonance in ε and μ (panels (b) and (c)). This situation results in two high-frequency band gaps (shaded zones) where the effective refractive index (panel (d)) is an imaginary or complex number. These band gap regions can move to higher frequencies if the separation between the wires is increased as in figure 7. Again, our theory correctly describes the system previously investigated by Pendry *et al* [24].

The regions of $\mathrm{Im}\,\mu(\omega) < 0$ in figures 6 and 7 should not be considered breaches of causality, but are associated with the fact that the wavelength $2\pi c/\omega$ is only $\sim$5 times as high as the lattice constant a. Thus, homogenization is not ideally applicable in this region, as argued in [36].

7.5. Doubly negative (left-handed) behavior

Now, we are going to focus our attention on the second (optical) pass-band in the case of cut wires (figures 6 and 7). In this spectral region, both ε and μ are real and negative. In

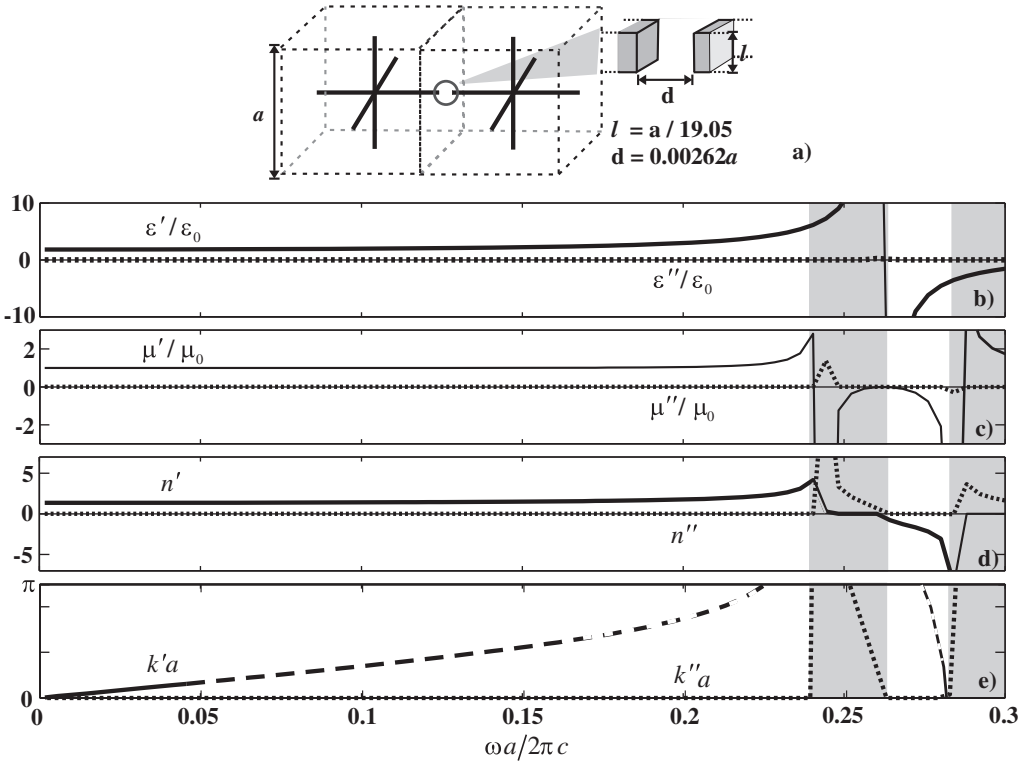

Figure 7. The same as figure 6 but with a larger gap between wires in neighboring cells. The behavior of the system is similar to that in figure 6 but is shifted to higher frequencies.

calculating n ($n = \pm\sqrt{\varepsilon\mu}$), we should take the negative sign of the square root as was pointed out by Veselago [22]. In this region, the metallo-dielectric PC has left-handed behavior as a consequence of the strong capacitance produced by the small gap between the wires and the induced eddy currents [68]. It is important to stress here that we have selected thin wires in order to shift the band gap to sufficiently low frequencies (long-wavelength limit). That is why we have chosen gaps as small as $d = 0.001\,05a$ and $d = 0.002\,62a$. The same *metamaterial* behavior can be found in similar systems with wider gaps and thicker wires. In figure 8, we can see the effect of severing the wires. When the wires are continuous the system behaves as a plasma-like effective medium with a low-frequency band gap characterized by an imaginary refractive index (panel (a)). A gap in the wires causes a qualitative change in the behavior at the macro-level and creates an acoustic pass-band where the index n is real and positive. This cut also creates a doubly negative region in the optical pass-band where n is real and negative (figure 6(d)). As the gap between the wires is increased (figure 7(d)), the same behavior is observed but shifted to higher frequencies.

We should remark here that the term *metamaterial* can also be applied to the system of 2D metallic wires studied in section 6. We have shown that this PC, composed of nonmagnetic materials, presents diamagnetic or paramagnetic behavior, depending on the polarization of the incident wave, being diamagnetic for the H-mode and paramagnetic for the E-mode.

Finally, it is important to stress that even though the figures shown in this section are based on formulae (59)–(62), obtained in the limit $k \to 0$, they can be reasonably used in the weakly nonlocal region where $|\mathbf{k}| < \pi/2a$.

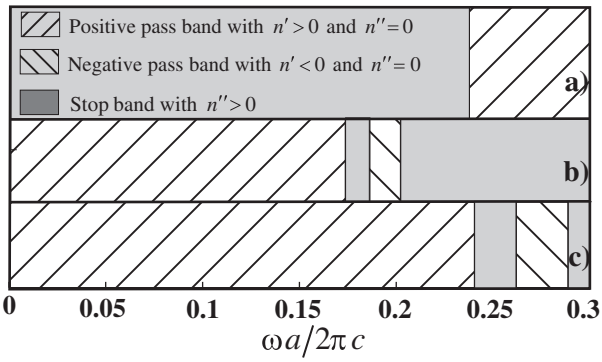

Figure 8. Summary of figures 5–7. The figure shows the effect of severing the wires in a PC of 3D metallic crosses in a cubic lattice. For continuous wires (a), the system presents a low-frequency band gap (plasma-like behavior). When the wires are cut (b), the plasma-like behavior disappears and the propagation of low-frequency waves is allowed. Cutting the wires also creates a region with a real and negative refractive index. When the gap is increased (c), the stop bands are shifted to higher frequencies, as is also the metamaterial region ($n < 0$).

8. Conclusion

We have developed a general homogenization theory for calculating the bulk electromagnetic response of a PC in the long-wavelength limit. By applying this mean-field theory, we derived analytic expressions (requiring matrix inversions) for the effective dyadics of both the usual dielectric response and the bianisotropic response, with these dyadics expressed in terms of the unit cell and Bravais lattice. These permittivity ($\overleftrightarrow{\boldsymbol{\varepsilon}}$), permeability ($\overleftrightarrow{\boldsymbol{\mu}}$) and crossed magneto-electric ($\overleftrightarrow{\boldsymbol{\gamma}}$, $\overleftrightarrow{\boldsymbol{\delta}}$) dyadics have all been expressed in terms of a basic conductivity dyadic ($\overleftrightarrow{\boldsymbol{\Sigma}}$), for which we have included two equivalent formulae: one gives a more physical understanding of the homogenization process and the other is more convenient from the computational point of view. Unlike the nonlocal dielectric response, the bianisotropic metamaterial response allows the magnetic properties to emerge at the macro-level. It also has the advantage that the dyadics $\overleftrightarrow{\boldsymbol{\varepsilon}}$, $\overleftrightarrow{\boldsymbol{\mu}}$, $\overleftrightarrow{\boldsymbol{\gamma}}$ and $\overleftrightarrow{\boldsymbol{\delta}}$ are independent of the magnitude of the wave vector (although they can depend, in general, on its direction). It is interesting that the permeability dyadic $\overleftrightarrow{\boldsymbol{\mu}}$ of the bianisotropic response diagonalizes in a coordinate system with one axis parallel to the wave vector $\mathbf{k}$. Therefore, the principal axes of the permittivity $\overleftrightarrow{\boldsymbol{\varepsilon}}$ and permeability $\overleftrightarrow{\boldsymbol{\mu}}$ dyadics, in general, do not coincide, high-symmetry configurations being the exception. This situation could lead to new results in the crystal optics of periodic composites. Within our homogenization theory, the crossed magneto-electric dyadics ($\overleftrightarrow{\boldsymbol{\gamma}}$, $\overleftrightarrow{\boldsymbol{\delta}}$) of the bianisotropic response vanish in the limit $k \to 0$ if the unit cell possesses inversion symmetry. Hence, in this important case the response is given entirely in terms of $\overleftrightarrow{\boldsymbol{\varepsilon}}$ and $\overleftrightarrow{\boldsymbol{\mu}}$. Even in this relatively simple situation, the physics of anisotropic metamaterials is still very rich (see, for example, Rosa *et al* [59, 69]). We have verified our theory by reducing our general results to those obtained in previous publications: analytically to the Maxwell–Garnett formula for small spheres and to the Pendry effective permittivity for a 3D system of metallic wires ('3D crosses') and numerically for dielectric 2D cylinders and 3D spheres. Moreover, we presented numerical results for metallo-dielectric

photonic crystals. In contrast with the pure dielectric case where there are no magnetic effects, we have found paramagnetic and diamagnetic behavior in 2D PCs of metallic wires, depending on the polarization—respectively parallel and perpendicular to the wires. We studied in detail, numerically, 3D systems of mutually perpendicular wires ('3D crosses'), focusing on the transition from continuous wires to cut wires and determining the effect of the width of the gap created between the severed wires. This leads to the disappearance of the low-frequency stop band (for the continuous wires) and its replacement by an 'acoustic' pass-band (for the cut wires). The second ('optical') pass-band is characterized by both the permittivity and the permeability being negative. This metamaterial behavior results from the capacitance created in the gaps between wires and the eddy currents induced by the magnetic field.

The theory presented in this paper bridges the gap between the PC or micro-level description and the uniform or macro-level description. It is based on first principles, characterizing the PC by means of a position-dependent generalized conductivity. It is a classical mean-field theory in the spirit of solid state theory. In principle, our final formulae for the bianisotropic response ($\overleftrightarrow{\boldsymbol{\varepsilon}}$, $\overleftrightarrow{\boldsymbol{\mu}}$, $\overleftrightarrow{\boldsymbol{\gamma}}$ and $\overleftrightarrow{\boldsymbol{\delta}}$) can be applied to 1D, 2D and 3D photonic crystals with arbitrary Bravais lattices and arbitrary composition of the unit cell. The ensuing numerical work involves matrix inversion and reciprocal lattice summation. On the downside, convergence can be slow, computer memory can be insufficient and computation times can be lengthy. For this reason, in the present lengthy paper we have avoided applications to PCs that lack inversion symmetry, postponing such calculations for future work.

The derived effective material dyadics $\overleftrightarrow{\boldsymbol{\varepsilon}}$, $\overleftrightarrow{\boldsymbol{\mu}}$, $\overleftrightarrow{\boldsymbol{\gamma}}$ and $\overleftrightarrow{\boldsymbol{\delta}}$ can depend on the frequency—not, however, on the magnitude of the Bloch wave vector $\mathbf{k}$. Nevertheless, this work could be readily generalized to first or second order in $|\mathbf{k}|$. In the case of 2D PCs, it should be interesting to investigate out-of-plane propagation. Finally, it should also be noted that the application of our formulae to the optical response (say, of a periodic composite slab) would also require long vacuum wavelength ($2\pi c/\omega \gg a$), in addition to long Bloch wavelengths ($2\pi/k \gg a$).

Acknowledgments

PH is grateful to D R Smith for introducing him to the bianisotropic response. This work was partially supported by CONACyT under grant numbers SEP-2004-C01-46425, 41195-F and 103644. JAR-A and UA-B are grateful to CONACyT for support of their doctoral studies.

Appendix A. Derivation of equation (25)

Let us rewrite the system of equations (19) in the form

$$\sum_{\mathbf{G}'} \overleftrightarrow{\mathbf{N}}(\mathbf{k};\mathbf{G},\mathbf{G}')\cdot\mathbf{e}(\mathbf{G}') = 0, \tag{A.1}$$

where

$$\overleftrightarrow{\mathbf{N}}(\mathbf{k};\mathbf{G},\mathbf{G}') = [(|\mathbf{k}+\mathbf{G}|^2 - k_0^2)\overleftrightarrow{\mathbf{I}} - (\mathbf{k}+\mathbf{G})(\mathbf{k}+\mathbf{G})]\delta_{\mathbf{G},\mathbf{G}'} - \mathrm{i}\omega\mu_0\hat{\sigma}(\mathbf{G}-\mathbf{G}')\overleftrightarrow{\mathbf{I}}. \tag{A.2}$$

Here, $\mathbf{G}$ and $\mathbf{G}'$ are vectors of the reciprocal lattice, including $\mathbf{G}=0$ and $\mathbf{G}'=0$. We can express $\overleftrightarrow{\boldsymbol{\Sigma}}(\mathbf{k})$ (equation (24)) in terms of the matrix $\overleftrightarrow{\mathbf{N}}$. Indeed, as follows from equation (A.2), the

Fourier coefficients of the conductivity, $\hat{\sigma}(\mathbf{G})$, are connected to $\overleftrightarrow{\mathbf{N}}$ as

$$\overleftrightarrow{\mathbf{N}}(\mathbf{k};0,0)-(k^2-k_0^2)\overleftrightarrow{\mathbf{I}}+\mathbf{kk}=-\mathrm{i}\omega\mu_0\hat{\sigma}(0)\overleftrightarrow{\mathbf{I}}, \tag{A.3}$$

$$\overleftrightarrow{\mathbf{N}}(\mathbf{k};0,\mathbf{G}')=-\mathrm{i}\omega\mu_0\hat{\sigma}(-\mathbf{G}')\overleftrightarrow{\mathbf{I}}, \quad \text{for} \quad \mathbf{G}'\neq 0, \tag{A.4}$$

$$\overleftrightarrow{\mathrm{N}}(\mathbf{k};\mathbf{G},0)=-\mathrm{i}\omega\mu_0\hat{\sigma}(\mathbf{G})\overleftrightarrow{\mathbf{I}}, \quad \text{for} \quad \mathbf{G}\neq 0. \tag{A.5}$$

Besides, as was recently demonstrated by one of us [60], there exists a relation between the inverse of a submatrix and the inverse of its original matrix. In the case at hand, $\overleftrightarrow{\mathbf{M}}$ is a submatrix of $\overleftrightarrow{\mathbf{N}}$, with the row $\mathbf{G}=0$ and the column $\underline{\mathbf{G}'=0}$ having been eliminated. From the aforementioned relation [60], it follows that

$$\overleftrightarrow{\mathbf{M}}^{-1}(\mathbf{k};\mathbf{G},\mathbf{G}')=\overleftrightarrow{\mathbf{N}}^{-1}(\mathbf{k};\mathbf{G},\mathbf{G}')-\overleftrightarrow{\mathbf{N}}^{-1}(\mathbf{k};\mathbf{G},0)\cdot\{\overleftrightarrow{\mathbf{N}}^{-1}(\mathbf{k};\mathbf{G},0)\}^{-1}\cdot\overleftrightarrow{\mathbf{N}}^{-1}(\mathbf{k};0,\mathbf{G}'). \tag{A.6}$$

In the above equation, $\overleftrightarrow{\mathbf{N}}^{-1}(\mathbf{k};\mathbf{G},\mathbf{G}')$ is the inverse of the matrix $\overleftrightarrow{\mathbf{N}}(\mathbf{k};\mathbf{G},\mathbf{G}')$ of infinite size, and $\{\overleftrightarrow{\mathbf{N}}^{-1}(\mathbf{k};0,0)\}^{-1}$ symbolizes the inverse of the 3×3 matrix block $\overleftrightarrow{\mathbf{N}}^{-1}(\mathbf{k};0,0)$.

Now, we can substitute equations (A.3)–(A.6) into (24). We obtain

$$\overleftrightarrow{\boldsymbol{\Sigma}}(\mathbf{k})=\frac{\mathrm{i}}{\omega\mu_0}\Bigg\{\overleftrightarrow{\mathbf{N}}(\mathbf{k};0,0)-(k^2-k_0^2)\overleftrightarrow{\mathbf{I}}+\mathbf{kk}-{\sum_{\mathbf{G},\mathbf{G}'}}'\overleftrightarrow{\mathbf{N}}(\mathbf{k};0,\mathbf{G})\cdot[\overleftrightarrow{\mathbf{N}}^{-1}(\mathbf{k};\mathbf{G},\mathbf{G}')$$
$$-\overleftrightarrow{\mathbf{N}}^{-1}(\mathbf{k};\mathbf{G},0)\cdot\{\overleftrightarrow{\mathbf{N}}^{-1}(\mathbf{k};0,0)\}^{-1}\cdot\overleftrightarrow{\mathbf{N}}^{-1}(\mathbf{k};0,\mathbf{G}')]\cdot\overleftrightarrow{\mathbf{N}}(\mathbf{k};\mathbf{G}',0)\Bigg\}. \tag{A.7}$$

We replace $\overleftrightarrow{\mathbf{N}}(\mathbf{k};0,\mathbf{G})$ by $\overleftrightarrow{\mathbf{N}}(\mathbf{k};\mathbf{G}',\mathbf{G})\delta_{\mathbf{G}'0}$ and $\overleftrightarrow{\mathbf{N}}^{-1}(\mathbf{k};\mathbf{G},0)$ by $\overleftrightarrow{\mathbf{N}}^{-1}(\mathbf{k};\mathbf{G},\mathbf{G}')\delta_{\mathbf{G}'0}$, which facilitates the summations over $\mathbf{G}$ and $\mathbf{G}'$. After some algebra we are left with the simple result

$$\overleftrightarrow{\boldsymbol{\Sigma}}(\mathbf{k})=\frac{\mathrm{i}}{\omega\mu_0}[\{\overleftrightarrow{\mathbf{N}}^{-1}(\mathbf{k};0,0)\}^{-1}-(k^2-k_0^2)\overleftrightarrow{\mathbf{I}}+\mathbf{kk}], \tag{A.8}$$

which is equation (25).

Appendix B. Expansion of $\overleftrightarrow{\boldsymbol{\Sigma}}(\mathbf{k})$ in powers of k

Let us rewrite the dyadic $\overleftrightarrow{\mathbf{M}}(\mathbf{k};\mathbf{G},\mathbf{G}')$ (equation (21)) as

$$\overleftrightarrow{\mathbf{M}}(\mathbf{k};\mathbf{G},\mathbf{G}')=\overleftrightarrow{\mathbf{M}}_0(\mathbf{G},\mathbf{G}')+k\overleftrightarrow{\mathbf{M}}_1(\mathbf{G},\mathbf{G}')+k^2\overleftrightarrow{\mathbf{M}}_2(\mathbf{G},\mathbf{G}'), \tag{B.1}$$

where

$$\begin{aligned}\overleftrightarrow{\mathbf{M}}_0(\mathbf{G},\mathbf{G}')&=[(\mathbf{G}^2-k_0^2)\overleftrightarrow{\mathbf{I}}-\mathbf{GG}]\delta_{\mathbf{G},\mathbf{G}'}-\mathrm{i}\omega\mu_0\hat{\sigma}(\mathbf{G}-\mathbf{G}')\overleftrightarrow{\mathbf{I}},\\ \overleftrightarrow{\mathbf{M}}_1(k;\mathbf{G},\mathbf{G}')&=\overleftrightarrow{\mathbf{L}}(\hat{\mathbf{k}},\mathbf{G})\delta_{\mathbf{G},\mathbf{G}'},\\ \overleftrightarrow{\mathbf{M}}_2(k^2;\mathbf{G},\mathbf{G}')&=[\overleftrightarrow{\mathbf{I}}-\hat{\mathbf{k}}\hat{\mathbf{k}}]\delta_{\mathbf{G},\mathbf{G}'}.\end{aligned} \tag{B.2}$$

Here, $\overleftrightarrow{\mathbf{L}}(\hat{\mathbf{k}},\mathbf{G})$ has been defined in equation (45). Using these definitions, we can write the inverse of the dyadic $\overleftrightarrow{\mathbf{M}}(\mathbf{k};\mathbf{G},\mathbf{G}')$ in the form

$$\overleftrightarrow{\mathbf{M}}^{-1}(\mathbf{k},\mathbf{G},\mathbf{G}')=[\overleftrightarrow{\mathbf{I}}\delta_{\mathbf{G}\mathbf{G}''}+\overleftrightarrow{\mathbf{M}}_0^{-1}(\mathbf{G},\mathbf{G}'')\cdot k\overleftrightarrow{\mathbf{M}}_1(\mathbf{G}'',\mathbf{G}''')$$
$$+\overleftrightarrow{\mathbf{M}}_0^{-1}(\mathbf{G},\mathbf{G}'')\cdot k^2\overleftrightarrow{\mathbf{M}}_2(\mathbf{G}'',\mathbf{G}''')]^{-1}\cdot\overleftrightarrow{\mathbf{M}}_0^{-1}(\mathbf{G}''',\mathbf{G}'). \tag{B.3}$$

Here, we have used the identity $(\mathbf{AB})^{-1} = \mathbf{B}^{-1}\mathbf{A}^{-1}$ and summation over repeated $\mathbf{G}'$s is implied. We develop the inverse dyadic in equation (B.3) in a Taylor expansion as $(\mathbf{I}+\mathbf{A})^{-1} = \mathbf{I}-\mathbf{A}+\mathbf{A}\cdots$. Then,

$$\begin{aligned}\overleftrightarrow{\mathbf{M}}^{-1}(\mathbf{k},\mathbf{G},\mathbf{G}') \cong{}& \overleftrightarrow{\mathbf{M}}_0^{-1}(\mathbf{G},\mathbf{G}') - \overleftrightarrow{\mathbf{M}}_0^{-1}(\mathbf{G},\mathbf{G}'')\cdot k\overleftrightarrow{\mathbf{M}}_1(\mathbf{G}'',\mathbf{G}''')\cdot\overleftrightarrow{\mathbf{M}}_0^{-1}(\mathbf{G}''',\mathbf{G}')\\ &- \overleftrightarrow{\mathbf{M}}_0^{-1}(\mathbf{G},\mathbf{G}'')\cdot k^2\overleftrightarrow{\mathbf{M}}_2(\mathbf{G}'',\mathbf{G}''')\cdot\overleftrightarrow{\mathbf{M}}_0^{-1}(\mathbf{G}''',\mathbf{G}') + \overleftrightarrow{\mathbf{M}}_0^{-1}(\mathbf{G},\mathbf{G}'')\cdot k\overleftrightarrow{\mathbf{M}}_1(\mathbf{G}'',\mathbf{G}''')\\ &\cdot\overleftrightarrow{\mathbf{M}}_0^{-1}(\mathbf{G}''',\mathbf{G}^{IV})\cdot k\overleftrightarrow{\mathbf{M}}_1(\mathbf{G}^{IV},\mathbf{G}^{V})\cdot\overleftrightarrow{\mathbf{M}}_0^{-1}(\mathbf{G}^{V},\mathbf{G}'). \qquad \text{(B.4)}\end{aligned}$$

In the above equation, we have neglected terms giving contributions of order higher than k^2. The expression just obtained for $\overleftrightarrow{\mathbf{M}}^{-1}(\mathbf{k};\mathbf{G},\mathbf{G}')$ can be verified by calculating $\overleftrightarrow{\mathbf{M}}(\mathbf{k};\mathbf{G},\mathbf{G}')\cdot\overleftrightarrow{\mathbf{M}}^{-1}(\mathbf{k};\mathbf{G},\mathbf{G}')$, which is equal to $\overleftrightarrow{\mathbf{I}}$ up to second-order terms. Substituting equation (B.4) into (24) and using the definitions given in equations (41) and (44), we obtain

$$\begin{aligned}\overleftrightarrow{\boldsymbol{\Sigma}}(\mathbf{k}) ={}& \hat{\sigma}(\mathbf{G}=0)\overleftrightarrow{\mathbf{I}} + \mathrm{i}\omega\mu_0 {\sum_{\mathbf{G}}}' \hat{\sigma}(\mathbf{G})\overleftrightarrow{\mathbf{C}}_1(\mathbf{G})\\ &- \mathrm{i}\omega\mu_0 k {\sum_{\mathbf{G}}}' \overleftrightarrow{\mathbf{C}}_1(\mathbf{G})\cdot\overleftrightarrow{\mathbf{L}}(\hat{\mathbf{k}},\mathbf{G})\cdot\overleftrightarrow{\mathbf{C}}_2(\mathbf{G}) - \mathrm{i}\omega\mu_0 k^2 {\sum_{\mathbf{G}}}' \overleftrightarrow{\mathbf{C}}_1(\mathbf{G})\cdot(\overleftrightarrow{\mathbf{I}}-\hat{\mathbf{k}}\hat{\mathbf{k}})\cdot\overleftrightarrow{\mathbf{C}}_2(\mathbf{G})\\ &+ \mathrm{i}\omega\mu_0 k^2 {\sum_{\mathbf{G},\mathbf{G}'}}' \overleftrightarrow{\mathbf{C}}_1(\mathbf{G})\cdot\overleftrightarrow{\mathbf{L}}(\hat{\mathbf{k}},\mathbf{G})\cdot\overleftrightarrow{\mathbf{M}}_0^{-1}(\mathbf{G},\mathbf{G}')\cdot\overleftrightarrow{\mathbf{L}}(\hat{\mathbf{k}},\mathbf{G}')\cdot\overleftrightarrow{\mathbf{C}}_2(\mathbf{G}'). \qquad \text{(B.5)}\end{aligned}$$

From equation (B.5) it is clear that the effective conductivity can be written as $\overleftrightarrow{\boldsymbol{\Sigma}}(\mathbf{k}) = \overleftrightarrow{\boldsymbol{\Sigma}}_0 + k\overleftrightarrow{\boldsymbol{\Sigma}}_1(\hat{\mathbf{k}}) + k^2\overleftrightarrow{\boldsymbol{\Sigma}}_2(\hat{\mathbf{k}})$, namely equation (37) with $\overleftrightarrow{\boldsymbol{\Sigma}}_0$, $\overleftrightarrow{\boldsymbol{\Sigma}}_1(\hat{\mathbf{k}})$ and $\overleftrightarrow{\boldsymbol{\Sigma}}_2(\hat{\mathbf{k}})$ defined by equations (40), (44) and (47), respectively.

Appendix C. Determination of $p = 1/2$ by imposing the Onsager symmetry relations

From the definition of the inverse of a matrix, we obtain the following three relations:

$${\sum_{\mathbf{G}'}}' \overleftrightarrow{\mathbf{M}}_0(\mathbf{G},\mathbf{G}')\cdot\overleftrightarrow{\mathbf{M}}_0^{-1}(\mathbf{G}',\mathbf{G}'') = \overleftrightarrow{\mathbf{I}}\delta_{\mathbf{G},\mathbf{G}''}, \qquad \text{(C.1)}$$

$${\sum_{\mathbf{G}'}}' \overleftrightarrow{\mathbf{M}}_0(-\mathbf{G},\mathbf{G}')\cdot\overleftrightarrow{\mathbf{M}}_0^{-1}(\mathbf{G}',-\mathbf{G}'') = \overleftrightarrow{\mathbf{I}}\delta_{\mathbf{G},\mathbf{G}''}, \qquad \text{(C.2)}$$

$${\sum_{\mathbf{G}'}}' \overleftrightarrow{\mathbf{M}}_0(-\mathbf{G},-\mathbf{G}')\cdot\overleftrightarrow{\mathbf{M}}_0^{-1}(-\mathbf{G}',-\mathbf{G}'') = \overleftrightarrow{\mathbf{I}}\delta_{\mathbf{G},\mathbf{G}''}. \qquad \text{(C.3)}$$

Besides, from equation (42) we can see that $\overleftrightarrow{\mathbf{M}}_0(-\mathbf{G},-\mathbf{G}') = \overleftrightarrow{\mathbf{M}}_0(\mathbf{G}',\mathbf{G})$ and $M_{0ij}(\mathbf{G},\mathbf{G}') = M_{0ji}(\mathbf{G},\mathbf{G}')$. Using these relations and equation (C.3), we obtain

$${\sum_{\mathbf{G}'}}' M_{0jk}^{-1}(-\mathbf{G}',-\mathbf{G}'')M_{0ji}(\mathbf{G}',\mathbf{G}) = \delta_{ik}\delta_{\mathbf{G},\mathbf{G}''}. \qquad \text{(C.4)}$$

The last equation implies that

$$M_{0jk}^{-1}(-\mathbf{G}',-\mathbf{G}'') = M_{0kj}^{-1}(\mathbf{G}'',\mathbf{G}'). \qquad \text{(C.5)}$$

Now, using the above derived properties of symmetry for $\overleftrightarrow{\mathbf{M}}_0^{-1}(\mathbf{G}', \mathbf{G}'')$, one can straightforwardly obtain

$$\overleftrightarrow{\boldsymbol{\Sigma}}_0 = \overleftrightarrow{\boldsymbol{\Sigma}}_0^{\mathrm{T}}, \qquad \overleftrightarrow{\boldsymbol{\Sigma}}_1 = -\overleftrightarrow{\boldsymbol{\Sigma}}_1^{\mathrm{T}}, \qquad \overleftrightarrow{\boldsymbol{\Sigma}}_2 = \overleftrightarrow{\boldsymbol{\Sigma}}_2^{\mathrm{T}}, \tag{C.6}$$

and consequently

$$\overleftrightarrow{\boldsymbol{\alpha}} = \overleftrightarrow{\boldsymbol{\alpha}}^{\mathrm{T}}, \qquad \overleftrightarrow{\boldsymbol{\beta}} = \overleftrightarrow{\boldsymbol{\varphi}}^{\mathrm{T}} \frac{(1-p)}{p}, \qquad \overleftrightarrow{\boldsymbol{\psi}} = \overleftrightarrow{\boldsymbol{\psi}}^{\mathrm{T}}. \tag{C.7}$$

The Onsager symmetry relations impose that

$$\overleftrightarrow{\boldsymbol{\delta}} = -\overleftrightarrow{\boldsymbol{\gamma}}^{\mathrm{T}}, \tag{C.8}$$

where the dyadics $\overleftrightarrow{\boldsymbol{\delta}}$ and $\overleftrightarrow{\boldsymbol{\gamma}}$ are given by equation (63). Substituting equation (C.7) into (63) and, in turn, into equation (C.8), we obtain $p = 1/2$.

Appendix D. Proof of equation (81)

The calculation of the matrix block $\overleftrightarrow{\mathbf{N}}^{-1}(\mathbf{k} = 0; 0, 0)$ is equivalent to solving the system of equations

$$\sum_{\mathbf{G}'} \{[(G^2 - k_0^2)\overleftrightarrow{\mathbf{I}} - \mathbf{GG}]\delta_{\mathbf{G},\mathbf{G}'} - \mathrm{i}\omega\mu_0\hat{\sigma}(\mathbf{G} - \mathbf{G}')\overleftrightarrow{\mathbf{I}}\} \cdot \overleftrightarrow{\mathbf{N}}^{-1}(\mathbf{k} = 0; \mathbf{G}', 0) = \delta_{\mathbf{G},0}\overleftrightarrow{\mathbf{I}}. \tag{D.1}$$

Using the transverse and longitudinal projection operators, $\overleftrightarrow{\mathbf{P}}_{\mathrm{T}}$ and $\overleftrightarrow{\mathbf{P}}_{\mathrm{L}}$, this equation can be rewritten as

$$[(G^2 - k_0^2)\overleftrightarrow{\mathbf{P}}_{\mathrm{T}}(\mathbf{G}) - k_0^2\overleftrightarrow{\mathbf{P}}_{\mathrm{L}}(\mathbf{G})] \cdot \overleftrightarrow{\mathbf{N}}^{-1}(\mathbf{k} = 0; \mathbf{G}, 0) - \mathrm{i}\omega\mu_0 \sum_{\mathbf{G}'} \hat{\sigma}(\mathbf{G} - \mathbf{G}')\overleftrightarrow{\mathbf{N}}^{-1}(\mathbf{k} = 0; \mathbf{G}', 0) = \delta_{\mathbf{G},0}\overleftrightarrow{\mathbf{I}}, \tag{D.2}$$

where $\overleftrightarrow{\mathbf{I}} = \overleftrightarrow{\mathbf{P}}_{\mathrm{T}}(\mathbf{G}) + \overleftrightarrow{\mathbf{P}}_{\mathrm{L}}(\mathbf{G})$, $\overleftrightarrow{\mathbf{P}}_{\mathrm{T}}(\mathbf{G}) = \overleftrightarrow{\mathbf{I}} - \hat{\mathbf{G}}\hat{\mathbf{G}}$ and $\mathbf{P}_{\mathrm{L}}(\mathbf{G}) = \hat{\mathbf{G}}\hat{\mathbf{G}}$. Now, we write the Fourier coefficients as follows:

$$\hat{\sigma}(\mathbf{G} - \mathbf{G}') = \hat{\sigma}_b\delta_{\mathbf{G},\mathbf{G}'} + \Delta\hat{\sigma}\,F(\mathbf{G} - \mathbf{G}'), \tag{D.3}$$

where $\Delta\hat{\sigma} = \hat{\sigma}_a - \hat{\sigma}_b$ and $F(\mathbf{G} - \mathbf{G}') = \frac{1}{A_{\mathrm{cu}}}\int_a \mathrm{e}^{-\mathrm{i}(\mathbf{G}-\mathbf{G}')\cdot r}\mathrm{d}\mathbf{r}$ is the inclusion form factor. Substituting equation (D.3) into (D.2), we obtain

$$[(G^2 - k_0^2 - \mathrm{i}\omega\mu_0\hat{\sigma}_b)\overleftrightarrow{\mathbf{P}}_{\mathrm{T}}(\mathbf{G}) - (k_0^2 + \mathrm{i}\omega\mu_0\hat{\sigma}_b)\overleftrightarrow{\mathbf{P}}_{\mathrm{L}}(\mathbf{G})] \cdot \overleftrightarrow{\mathbf{N}}^{-1}(\mathbf{k} = 0; \mathbf{G}, 0) - \mathrm{i}\omega\mu_0 \sum_{\mathbf{G}'} \Delta\hat{\sigma}\,F(\mathbf{G} - \mathbf{G}')\overleftrightarrow{\mathbf{N}}^{-1}(\mathbf{k} = 0; \mathbf{G}', 0) = \delta_{\mathbf{G},0}\overleftrightarrow{\mathbf{I}}. \tag{D.4}$$

This equation can be rewritten as

$$\overleftrightarrow{\mathbf{N}}^{-1}(\mathbf{k} = 0; \mathbf{G}, 0) - \mathrm{i}\omega\mu_0\Delta\hat{\sigma}\overleftrightarrow{\mathbf{O}}(\mathbf{G}) \sum_{\mathbf{G}'} F(\mathbf{G} - \mathbf{G}')\overleftrightarrow{\mathbf{N}}^{-1}(\mathbf{k} = 0; \mathbf{G}', 0) = \overleftrightarrow{\mathbf{O}}\delta_{\mathbf{G},0}, \tag{D.5}$$

where we have introduced the matrix $\overleftrightarrow{\mathbf{O}}(\mathbf{G})$:

$$\overleftrightarrow{\mathbf{O}}(\mathbf{G}) = \left[\frac{\overleftrightarrow{\mathbf{P}}_{\mathrm{T}}(\mathbf{G})}{G^2 - k_0^2 - \mathrm{i}\omega\mu_0\hat{\sigma}_b} - \frac{\overleftrightarrow{\mathbf{P}}_{\mathrm{L}}(\mathbf{G})}{k_0^2 + \mathrm{i}\omega\mu_0\hat{\sigma}_b}\right]. \tag{D.6}$$

From equation (D.5), it follows that $\overleftrightarrow{\mathbf{N}}^{-1}(\mathbf{k}=0;0,0)$ is related to the sum

$$\overleftrightarrow{\mathbf{C}}_0 = \sum_{\mathbf{G}'} F(-\mathbf{G}')\overleftrightarrow{\mathbf{N}}^{-1}(\mathbf{k}=0;\mathbf{G}',0), \tag{D.7}$$

according to

$$\overleftrightarrow{\mathbf{N}}^{-1}(\mathbf{k}=0;0,0) - \mathrm{i}\omega\mu_0\Delta\hat{\sigma}\overleftrightarrow{\mathbf{O}}(0)\sum_{\mathbf{G}'} F(-\mathbf{G}')\overleftrightarrow{\mathbf{N}}^{-1}(\mathbf{k}=0;\mathbf{G}',0) = \overleftrightarrow{\mathbf{O}}(0). \tag{D.8}$$

Multiplying equation (D.5) by $F(-\mathbf{G})$ and summing both sides over $\mathbf{G}$, we also find that

$$\sum_{\mathbf{G}'} F(-\mathbf{G})\overleftrightarrow{\mathbf{N}}^{-1}(\mathbf{k}=0;\mathbf{G},0) - \mathrm{i}\omega\mu_0\Delta\hat{\sigma}\sum_{\mathbf{G},\mathbf{G}'} F(-\mathbf{G})\overleftrightarrow{\mathbf{O}}(\mathbf{G})F(\mathbf{G}-\mathbf{G}')\overleftrightarrow{\mathbf{N}}^{-1}(\mathbf{k}=0;\mathbf{G}',0)$$
$$= F(0)\overleftrightarrow{\mathbf{O}}(0). \tag{D.9}$$

If we consider small inclusions ($f \ll 1$), then $F(\mathbf{G}-\mathbf{G}')$ is a function that slowly varies with the magnitude of $\mathbf{G}-\mathbf{G}'$. Hence, for $G \ll 1/r$, where r is the characteristic size of the inclusion, we can use the following approximation:

$$F(\mathbf{G}-\mathbf{G}') \approx F(0-\mathbf{G}') \approx F(-\mathbf{G}'). \tag{D.10}$$

This approximation is good enough to solve equation (D.9) because the dyadic $F(-\mathbf{G})\overleftrightarrow{\mathbf{O}}(\mathbf{G})$ therein decreases with G (see equation (D.6)) and practically vanishes at $Gr \gg 1$. Then, employing (D.7), (D.9) and (D.10), we obtain

$$\overleftrightarrow{\mathbf{C}}_0 - \mathrm{i}\omega\mu_0\sum_{\mathbf{G}} F(-\mathbf{G})\overleftrightarrow{\mathbf{O}}(\mathbf{G})\Delta\hat{\sigma}\overleftrightarrow{\mathbf{C}}_0 = \overleftrightarrow{\mathbf{O}}(0)F(0). \tag{D.11}$$

The solution of this equation can be written as

$$\overleftrightarrow{\mathbf{C}}_0 = \left[\overleftrightarrow{\mathbf{I}} - \mathrm{i}\omega\mu_0\Delta\hat{\sigma}\sum_{\mathbf{G}} F(-\mathbf{G})\overleftrightarrow{\mathbf{O}}(\mathbf{G})\right]^{-1}\cdot\overleftrightarrow{\mathbf{O}}(0)F(0), \tag{D.12}$$

which requires the calculation of the sum

$$\sum_{\mathbf{G}} F(-\mathbf{G}')\overleftrightarrow{\mathbf{O}}(\mathbf{G}) = \sum_{\mathbf{G}} F(-\mathbf{G})\left[\frac{\overleftrightarrow{\mathbf{I}} - (\mathbf{GG}/G^2)}{G^2 - k_0^2 - \mathrm{i}\omega\mu_0\hat{\sigma}_b} - \frac{(\mathbf{GG}/G^2)}{k_0^2 + \mathrm{i}\omega\mu_0\hat{\sigma}_b}\right]. \tag{D.13}$$

Since our formulae are being derived in the limit $k \to 0$, the term with $\mathbf{G}=0$ in equation (D.13) turns out to be equal to $-F(0)\overleftrightarrow{\mathbf{I}}/(k_0^2 + \mathrm{i}\omega\mu_0\hat{\sigma}_b)$.

In the long-wavelength limit, i.e. when $G/k_0 \gg 1$, the sum (D.13) can be simplified. Indeed, let us rewrite it as

$$\sum_{\mathbf{G}} F(-\mathbf{G})\overleftrightarrow{\mathbf{O}}(\mathbf{G}) = -\frac{F(0)\overleftrightarrow{\mathbf{I}}}{k_0^2 + \mathrm{i}\omega\mu_0\hat{\sigma}_b} + \sum_{\mathbf{G}'\neq 0}\frac{F(-G)(\overleftrightarrow{\mathbf{I}} - \mathbf{GG}/G^2)}{G^2 - k_0^2 - \mathrm{i}\omega\mu_0\hat{\sigma}_b} - \sum_{\mathbf{G}'\neq 0}\frac{F(-G)\mathbf{GG}/G^2}{k_0^2 + \mathrm{i}\omega\mu_0\hat{\sigma}_b}. \tag{D.14}$$

The second term on the right-hand side of equation (D.14) is much smaller than the others as $|k_0^2 + \mathrm{i}\omega\mu_0\hat{\sigma}_b| \ll G^2$. If the latter inequality is satisfied, we can write

$$\sum_{\mathbf{G}} F(-\mathbf{G})\overleftrightarrow{\mathbf{O}}(\mathbf{G}) \approx -\frac{F(0)\overleftrightarrow{\mathbf{I}}}{k_0^2 + \mathrm{i}\omega\mu_0\hat{\sigma}_b} - \sum_{\mathbf{G}'\neq 0} \frac{F(-G)\mathbf{GG}/G^2}{k_0^2 + \mathrm{i}\omega\mu_0\hat{\sigma}_b}. \tag{D.15}$$

Now, we should use the sum rules:

$$\sum_{\mathbf{G}\neq 0} F(-\mathbf{G}) = 1 - F(0), \tag{D.16}$$

and, for a cubic system,

$$\sum_{\mathbf{G}\neq 0} \frac{\mathbf{GG}}{G^2} F(-G) = \overleftrightarrow{\mathbf{I}}\frac{1}{3}\sum_{\mathbf{G}\neq 0} F(-\mathbf{G}') = \frac{1 - F(0)}{3}\overleftrightarrow{\mathbf{I}}. \tag{D.17}$$

Substituting equation (D.17) into (D.15), we finally obtain

$$\sum_{\mathbf{G}} F(-\mathbf{G}')\overleftrightarrow{\mathbf{O}}(\mathbf{G}) \cong \overleftrightarrow{\mathbf{I}}\left\{\frac{\frac{2}{3}F(0)}{-k_0^2 - \mathrm{i}\omega\mu_0\hat{\sigma}_b} - \frac{1}{3}\frac{1}{k_0^2 + \mathrm{i}\omega\mu_0\hat{\sigma}_b}\right\}. \tag{D.18}$$

Using equation (D.18), the expression for $\overleftrightarrow{\mathbf{C}}_0$ acquires the form

$$\overleftrightarrow{\mathbf{C}}_0 = \left[1 - \mathrm{i}\omega\mu_0\Delta\hat{\sigma}\left\{\frac{\frac{2}{3}f}{-k_0^2 - \mathrm{i}\omega\mu_0\hat{\sigma}_b} - \frac{1}{3}\frac{1}{k_0^2 + \mathrm{i}\omega\mu_0\hat{\sigma}_b}\right\}\right]^{-1}\left[\frac{\overleftrightarrow{\mathbf{I}}}{-k_0^2 - \mathrm{i}\omega\mu_0\hat{\sigma}_b}\right] f, \tag{D.19}$$

where $f = F(0)$. Simplifying,

$$\overleftrightarrow{\mathbf{C}}_0 = -\frac{f\overleftrightarrow{\mathbf{I}}}{k_0^2 + \mathrm{i}\omega\mu_0\left[\left(\hat{\sigma}_a - \hat{\sigma}_b\right)\left(\frac{2}{3}f + \frac{1}{3}\right) + \hat{\sigma}_b\right]}. \tag{D.20}$$

Finally, we substitute this result for $\overleftrightarrow{\mathbf{C}}_0$ into equation (D.8) and obtain

$$\overleftrightarrow{\mathbf{N}}^{-1}(\mathbf{k} = 0; 0, 0) = -\frac{1}{k_0^2 + \mathrm{i}\omega\mu_0\hat{\sigma}_b}\left(1 - \frac{\mathrm{i}\omega\mu_0(\hat{\sigma}_a - \hat{\sigma}_b)f}{k_0^2 + \mathrm{i}\omega\mu_0\left[\left(\hat{\sigma}_a - \hat{\sigma}_b\right)\left(\frac{2}{3}f + \frac{1}{3}\right) + \hat{\sigma}_b\right]}\right)\overleftrightarrow{\mathbf{I}}. \tag{D.21}$$

This is the desired result, equation (81).

Appendix E. Proof of equation (84)

Consider a plane wave with $\mathbf{k} = k_x\hat{\mathbf{x}}$ and $\mathbf{E} = E_z\hat{\mathbf{z}}$ traveling through a PC constructed with thin metallic wires that are parallel to the x, y and z coordinate axes ('3D crosses'). In this case, the 'active wires' are those parallel to $\hat{\mathbf{z}}$ direction and the contribution of the wires parallel to the $\hat{\mathbf{x}}$ and $\hat{\mathbf{y}}$ directions to the effective response can be neglected. This situation is equivalent to the calculation of the effective permittivity ε_{zz} of a 2D PC of thin metallic wires. By the way, in such a 2D PC, we can observe that the contribution of thin wires, parallel to the z direction, to the effective permittivity $\varepsilon_\perp$ is indeed negligible (see figure 5 and [33] and [49]). Then $\mathbf{G}(\mathrm{G}_x, G_y, 0) = \mathbf{G}(\mathrm{G}_\perp, 0)$ and

$$\hat{\sigma}(\mathbf{G} - \mathbf{G}') = \hat{\sigma}_a F(\mathbf{G} - \mathbf{G}') = \sigma F(\mathbf{G} - \mathbf{G}'), \tag{E.1}$$

where σ is the usual conductivity, $F(\mathbf{G}-\mathbf{G}') = \frac{1}{A_{\rm cu}}\int_a \mathrm{e}^{-\mathrm{i}(\mathbf{G}-\mathbf{G}')\cdot r}\,\mathrm{d}\mathbf{r}$ is the inclusion form factor and vacuum has been considered as the host medium. To obtain ε_{zz}, we derive from equation (D.1)

$$\overleftrightarrow{\mathbf{N}}_{zz}^{-1}(\mathbf{k}=0;\mathbf{G}_\perp,0) - \frac{\mathrm{i}\omega\mu_0\sigma}{G_\perp^2-k_0^2}\sum_{\mathbf{G}'_\perp} F(\mathbf{G}_\perp-\mathbf{G}'_\perp)\overleftrightarrow{\mathbf{N}}_{zz}^{-1}(\mathbf{k}=0;\mathbf{G}'_\perp,0) = -\frac{\delta_{\mathbf{G},0}}{k_0^2}. \tag{E.2}$$

Since the wires are assumed to be very thin, we can use the same approach as in equation (D.10) and rewrite equation (E.2) as

$$\overleftrightarrow{\mathbf{N}}_{zz}^{-1}(\mathbf{k}=0;\mathbf{G}_\perp,0) - \frac{\mathrm{i}\omega\mu_0\sigma}{G_\perp^2-k_0^2}C = -\frac{\delta_{\mathbf{G},0}}{k_0^2}, \tag{E.3}$$

where

$$C = \sum_{\mathbf{G}'_\perp} F(-\mathbf{G}'_\perp)\overleftrightarrow{\mathbf{N}}_{zz}^{-1}(\mathbf{k}=0;\mathbf{G}'_\perp,0). \tag{E.4}$$

Using the last equation, we obtain from equation (E.3)

$$C - \mathrm{i}\omega\mu_0\sigma\sum_{\mathbf{G}_\perp}\frac{F(-\mathbf{G}_\perp)}{G_\perp^2-k_0^2}C = -\frac{F(0)}{k_0^2}. \tag{E.5}$$

In the long-wavelength limit, i.e. when $G_\perp \gg k_0$, equation (E.5) is rewritten in the form

$$C = \left[1+\frac{\mathrm{i}\omega\mu_0\sigma F(0)}{k_0^2} - \mathrm{i}\omega\mu_0\sigma\sum_{\mathbf{G}'_\perp\neq 0}\frac{F(-\mathbf{G}'_\perp)}{\mathbf{G}_\perp^2}\right]^{-1}\left(-\frac{F(0)}{k_0^2}\right). \tag{E.6}$$

Substituting equation (E.6) into (E.3), we obtain

$$\overleftrightarrow{\mathbf{N}}_{zz}^{-1}(\mathbf{k}=0;0,0) = -\frac{1}{k_0^2}+\frac{\mathrm{i}\omega\mu_0\sigma}{k_0^2}\frac{F(0)}{k_0^2\left[1+\frac{\mathrm{i}\omega\mu_0\sigma F(0)}{k_0^2}-\mathrm{i}\omega\mu_0\sigma\sum\limits_{\mathbf{G}'_\perp\neq 0}\frac{F(-\mathbf{G}'_\perp)}{\mathbf{G}_\perp^2}\right]}. \tag{E.7}$$

After some algebraic manipulation, we obtain

$$\left\{\overleftrightarrow{\mathbf{N}}_{zz}^{-1}(0,0)\right\}^{-1} = 1-\frac{\mathrm{i}\omega\mu_0\sigma k_0^2 F(0)}{k_0^2-\mathrm{i}\omega\mu_0\sigma k_0^2\sum\limits_{\mathbf{G}_\perp\neq 0}F(-\mathbf{G}_\perp)/G_\perp^2}. \tag{E.8}$$

Substituting equation (E.8) into (43), we find that

$$\varepsilon_{\rm eff} = \varepsilon_0\left[1-\frac{\mu_0\sigma c^2 F(0)}{\mathrm{i}\omega+\mu_0\sigma\omega^2\sum\limits_{\mathbf{G}_\perp\neq 0}\frac{F(-\mathbf{G}_\perp)}{G_\perp^2}}\right]. \tag{E.9}$$

If we consider wires of circular cross-section, then

$$\sum_{\mathbf{G}_\perp\neq 0}\frac{F(-\mathbf{G}_\perp)}{G_\perp^2} = 2f\sum_{\mathbf{G}_\perp\neq 0}\frac{J_1(G_\perp r_0)}{G_\perp^3 r_0}, \tag{E.10}$$

where $f=\pi r_0^2/a^2$ is the filling fraction and $J_1(G_\perp r_0)$ is the first-order Bessel function. Considering that the function $J_1(G_\perp r_0)/G_\perp r_0$ is a smooth function for $G_\perp r_0 < 1$ and rapidly decreases for $G_\perp r_0 > 1$, we shall neglect the contribution of vectors with $G_\perp r_0 > 1$ in

equation (E.10). Besides, the function $J_1(G_\perp r_0)/G_\perp r_0$ will be approximated by the value of $1/2$ for $G_\perp r_0 < 1$. Then,

$$\sum_{\mathbf{G}_\perp \neq 0} \frac{F(-\mathbf{G}_\perp)}{G_\perp^2} \approx f \sum_{G_\perp \neq 0, G_\perp \leqslant 1/r_0} \frac{1}{G_\perp^2} \approx \frac{f}{(2\pi/a)^2} \int_0^{2\pi} \mathrm{d}\varphi \int_1^{a/2\pi r_0} \frac{g\,\mathrm{d}g}{g^2}$$

$$= \frac{fa^2}{2\pi} \ln\left(\frac{a}{2\pi r_0}\right) \approx \frac{fa^2}{2\pi} \ln\left(\frac{a}{r_0}\right), \tag{E.11}$$

where $g = G_\perp a/2\pi$. Note that the latter approximation in equation (E.11) is valid because of the assumption $(a/r_0) \gg 1$ and, then, $\ln(a/r_0) \gg \ln(2\pi)$. It means that the result (E.11) is not significantly altered by the choice of the cut-off value ($\sim 1/r_0$) for the sum over $\mathbf{G}_\perp$.

Finally, substituting equation (E.11) into equation (E.9), we find that

$$\varepsilon_{\mathrm{eff}} = \varepsilon_0 \left(1 - \frac{\frac{2\pi}{a^2}\frac{c^2}{\ln(a/r_0)}}{\omega^2 + \mathrm{i}\frac{\omega\varepsilon_0 c^2 2\pi}{\sigma f a^2 \ln(a/r_0)}}\right), \tag{E.12}$$

which is equation (84). In a similar way, the corresponding expression for wires with square cross-section is obtained as

$$\varepsilon_{\mathrm{eff}} = \varepsilon_0 \left(1 - \frac{\frac{2\pi}{a^2}\frac{c^2}{\ln(a/l)}}{\omega^2 + \mathrm{i}\frac{\omega\varepsilon_0 c^2 2\pi}{\sigma f a^2 \ln(a/l)}}\right), \tag{E.13}$$

where l is the side size of the square and $f = l^2/a^2$.

References

[1] Joannopoulos J D, Meade R D and Winn J N 2008 *Photonic Crystals: Molding the Flow of Light* 2nd edn (Princeton, NJ: Princeton University Press)
[2] Fink Y, Winn J N, Fan S, Chen C, Michel J, Joannopoulos J D and Thomas E L 1998 *Science* **282** 1679
[3] Chow E, Lin S Y, Wendt J R, Johnson S G and Joannopoulos J D 2001 *Opt. Lett.* **26** 286
[4] Asakawa K *et al* 2006 *New J. Phys.* **8** 208
[5] Loncar M, Yoshie T, Scherer A, Gogna P and Qiu Y 2002 *Appl. Phys. Lett.* **81** 2680
[6] Landau L D and Lifshitz E M 2004 *Electrodynamics of Continuous Media* (Amsterdam: Elsevier)
[7] Jackson J D 1975 *Classical Electrodynamics* (New York: Wiley)
[8] Lin S-Y, Hietala V M, Wang L and Jones E D 1996 *Opt. Lett.* **21** 1771
[9] Kosaka H, Kawashima T, Tomitama A, Tamamura M N, Sato T and Kawakami S 1998 *Phys. Rev.* B **58** R10096
[10] Halevi P, Krokhin A A and Arriaga J 1999 *Phys. Rev. Lett.* **82** 719
[11] Smith D R, Padilla W J, Vier D C, Nemat-Nasser S C and Schultz S 2000 *Phys. Rev. Lett.* **84** 4184
[12] Shelby R A, Smith D R, Nemat-Nasser S C and Schultz S 2001 *Appl. Phys. Lett.* **78** 489
[13] Shelby R A, Smith D R and Schultz S 2001 *Science* **292** 77
[14] Agranovich V M and Gartstein Y N 2006 *Phys.—Usp.* **49** 1029
[15] Schuster A 1909 *An Introduction to the Theory of Optics* 2nd edn (London: E Arnold)
[16] Mandel'shtam L I 1945 *Zh. Eksp. Teor. Fiz.* **15** 475
[17] Mandel'shtam L I 1972 *Lektsii po Optike, Teorii Otnositel'nosti i Kvantovoi Mekhanike (Lectures on Optics, Relativity, and Quantum Mechanics)* (Moscow: Nauka)
[18] Sivukhin D V 1957 *Opt. Spectrosc.* **3** 308
[19] Pafomov V E 1956 *Zh. Eksp. Teor. Fiz.* **30** 761
Pafomov V E 1956 *Sov. Phys.—JETP* **5** 597

[20] Pafomov V E 1957 *Zh. Eksp. Teor. Fiz.* **33** 1074
Pafomov V E 1958 *Sov. Phys.—JETP* **6** 806
[21] Pafomov V E 1959 *Zh. Eksp. Teor. Fiz.* **36** 1853
Pafomov V E 1959 *Sov. Phys.—JETP* **9** 1321
[22] Veselago V G 1967 *Usp. Fiz. Nauk* **92** 517
Veselago V G 1968 *Sov. Phys.—Usp.* **10** 509
[23] Pendry J B, Holden A J, Stewart W J and Youngs I 1996 *Phys. Rev. Lett.* **76** 4773
[24] Pendry J B, Holden A J, Robbins D J and Stewart W J 1999 *IEEE Trans. Microw. Theory Tech.* **47** 2075
[25] Ishimaru A, Lee S, Kuga Y and Jandhyala V 2003 *IEEE Trans. Antenna Propag.* **51** 2551
[26] Belov P A and Simovski C R 2005 *Phys. Rev.* E **72** 026615
[27] Lamb W, Wood D M and Ashcroft N W 1980 *Phys. Rev.* B **21** 2248
[28] Felbacq D and Bouchitté G 2005 *Opt. Lett.* **30** 1189
[29] Eleftheriades G V and Kremer P C 2002 *IEEE Trans. Microw. Theory Tech.* **50** 2703
[30] Tao R, Chen Z and Sheng P 1990 *Phys. Rev.* B **41** 2417
[31] Datta S, Chan C T, Ho K M and Soukoulis C M 1993 *Phys. Rev.* B **48** 14936
[32] Krokhin A A, Halevi P and Arriaga J 2002 *Phys. Rev.* B **65** 115208
[33] Krokhin A A, Reyes E and Gumen L 2007 *Phys. Rev.* B **75** 045131
[34] Chui S T and Lin Z 2008 *Phys. Rev.* E **78** 065601
[35] Smith D R, Vier D C, Koschny Th and Soukoulis C M 2005 *Phys. Rev.* E **71** 036617
[36] Koschny T, Markoš P, Economou E N, Smith D R, Vier D C and Soukoulis C M 2005 *Phys. Rev.* B **71** 245105
[37] Chen X, Wu B, Kong J and Grzegorczyk T M 2005 *Phys. Rev.* E **71** 046610
[38] Simovski C R and Tretyakov S A 2007 *Phys. Rev.* B **75** 195111
[39] Menzel C, Rockstuhl C, Paul T and Lederer F 2008 *Phys. Rev.* B **77** 195328
[40] Plum E, Zhou J, Dong J, Fedotov V A, Koschny T, Soukoulis C M and Zheludev N I 2009 *Phys. Rev.* B **79** 035407
[41] Romero I and García de Abajo F J 2009 *Opt. Express* **17** 22012
[42] Smith D R, Vier D C, Kroll N and Schultz S 2000 *Appl. Phys. Lett.* **77** 2246
[43] Smith D R and Pendry J B 2006 *J. Opt. Soc. Am.* B **23** 391
[44] Tsukerman I 2011 *J. Opt. Soc. Am.* B **28** 577
[45] Silveirinha M G and Fernandes C A 2005 *IEEE Trans. Antennas Propag.* **53** 59
[46] Silveirinha M G and Fernandes C A 2005 *IEEE Trans. Microw. Theory Tech.* **53** 1418
[47] Silveirinha M G 2006 *Phys. Rev.* E **73** 046612
[48] Silveirinha M G 2007 *Phys. Rev.* B **75** 115104
[49] Silveirinha M G 2007 *Phys. Rev.* B **76** 245117
[50] Costa J T, Silveirinha M G and Maslovski S I 2009 *Phys. Rev.* B **80** 235124
[51] Căbuz A I, Felbacq D and Cassagne D 2007 *Phys. Rev. Lett.* **98** 037403
[52] Mackay T G, Lakhtakia A and Weiglhofer W S 2000 *Phys. Rev.* E **62** 6052
[53] Eberhard J P 2005 *Phys. Rev.* E **72** 036616
[54] Mochán W L and Barrera R G 1985 *Phys. Rev.* B **32** 4984
[55] Ortiz G P, Martínez-Zérega B E, Mendoza B S and Mochán W L 2009 *Phys. Rev.* B **79** 245132
[56] Fietz C and Shvets G 2010 *Physica* B **405** 2930
[57] Condon E U 1937 *Rev. Mod. Phys.* **9** 432
[58] Hornreich R M and Shtrikman S 1968 *Phys. Rev.* **171** 1065
[59] Rosa F S S, Dalvit D A R and Milonni P W 2008 *Phys. Rev.* A **78** 032117
[60] Cerdán-Ramírez V, Zenteno-Mateo B, Sampedro M P, Palomino-Ovando M A, Flores-Desirena B and Pérez-Rodríguez F 2009 *J. Appl. Phys.* **106** 103520
[61] Agranovich V M and Ginzburg V L 1984 *Crystal Optics with Spatial Dispersion, and Exitons* (*Springer Series in Solid State Sciences* vol 42) (Berlin: Springer)
[62] Agranovich V M, Shen Y R, Baughman R H and Zakhidov A A 2004 *Phys. Rev.* B **69** 165112

[63] Fuchs R and Halevi P 1992 Introductory chapter *Spatial Dispersion in Solids and Plasmas* ed P Halevi (Amsterdam: Elsevier)
[64] Landau L D and Lifshitz E M 1984 *Statistical Physics* ed L D Landau and E M Lifshitz (*Course in Theoretical Physics* vol 5) (Oxford: Elsevier Butterworth–Heinemann)
[65] Amirkhizi V and Nemat-Nasser S 2008 *C. R. Mec.* **336** 24
[66] Pendry J B, Holden A J, Robbins D J and Stewart W J 1998 *J. Phys.: Condens. Matter* **10** 4785
[67] Silveirinha M G 2009 *Phys. Rev.* B **79** 035118
[68] Pendry J B and Smith D R 2004 *Phys. Today* **57** 37
[69] Rosa F S S, Dalvit D A R and Milonni P W 2008 *Phys. Rev. Lett.* **100** 183602